UCLA-ENG-81-101
MARCH 1981

THE VELOCITY FIELD NEAR THE ORIFICE OF A HELMHOLTZ RESONATOR IN GRAZING FLOW

ANDREW F. CHARWAT
BRUCE E. WALKER

UCLA • SCHOOL OF ENGINEERING AND APPLIED SCIENCE

ABSTRACT

Detailed measurements of the time-dependent velocities induced inside and outside the opening of an acoustically excited, two-dimensional Helmholtz resonator imbedded in a grazing flow are presented. The remarkably clear structure of the perturbation field which evokes a pulsating source and a coherently pulsating vortex-immage pair is described. The simple phenomemological "lid-model" which correlates the variation in the components of the acoustic impedance with the velocity of the grazing flow is discussed an extended.

INTRODUCTION

Acoustically excited cavities (Helmholtz resonators) exhibit a marked increase in acoustic resistance and a decrease in reactance when there is grazing flow over the cavity. The phenomenon is well documented experimentally [1][2] for a variety of configuations of the resonator orifice, excitation levels and grazing velocities. However, there are only a few studies of the flow-field in and around the orifice which could serve as a basis for a physical interpretation of the interaction between the acoustic field and the outer flow. Baumeister and Rice [3] used dye-visualization techniques to outline the flow in and out of orifice in the boundary of a water channel. Ingard and coworkers [4,5] provided insight into the structure of the flow associated with the pulsating jet issuing out of the cavity but their experiments involve no external flow over the orifice. Rice [5] and Rogers and Hersh [7] proposed phenomenological models which portray the behavior of the acoustic resistance resonably well; however, the observed changes in the inertance have eluded satisfactory explanation.

The objective of the present study is to map out the velocity field in the neighborhood of the orifice of a resonator imbedded in grazing flow. In order to facilitate the interpretation a two-dimensional configuration, i.e., a high aspect-ratio slot was studied, instead of the usual circular orifice. The principal independent variable is the velocity of the grazing flow; the frequency and level of the acoustic excitation are constant. The components of the vector

velocity on a dense array of points in and above the resonator were obtained throughout the cycle and yielded a remarkably coherent picture. A large amount of data is involved, of which only examples illustrating the basic structure of the field are given in this paper. A more complete compilation of results is published in a separate report[8].

The impedance of the two-dimensional test resonator determined by standard acoustic measurements of the amplitude and phase of the pressure incident on the surface of the orifice compared to that inside the resonator cavity is shown as a function of the grazing velocity in figure 1. The resistance and reactance follow the known trends for resonators with three-dimensional (circular) orifices except that the rate of increase in the resistance with the velocity of the grazing flow is larger by a factor of almost two. These characteristics are insensitive to the level and frequency of the excitation. Figure 1 also shows points calculated from the incident pressure and the space-averaged normal velocity (volume flow) obtained by integrating the measurements along a plane immediately above the opening. The second result is not as accurate as that obtained from the two-microphone method but the accord between the two methods is satisfactory.

A description of the experimental procedure follows. The results are then presented in two ways: as maps of the perturbation field and as trajectories of imaginary particles through the flow. A model describing the perturbation field by a pulsating source coupled to a pulsating vortex pair is suggested; this, in effect, is an extension

FIGURE 1

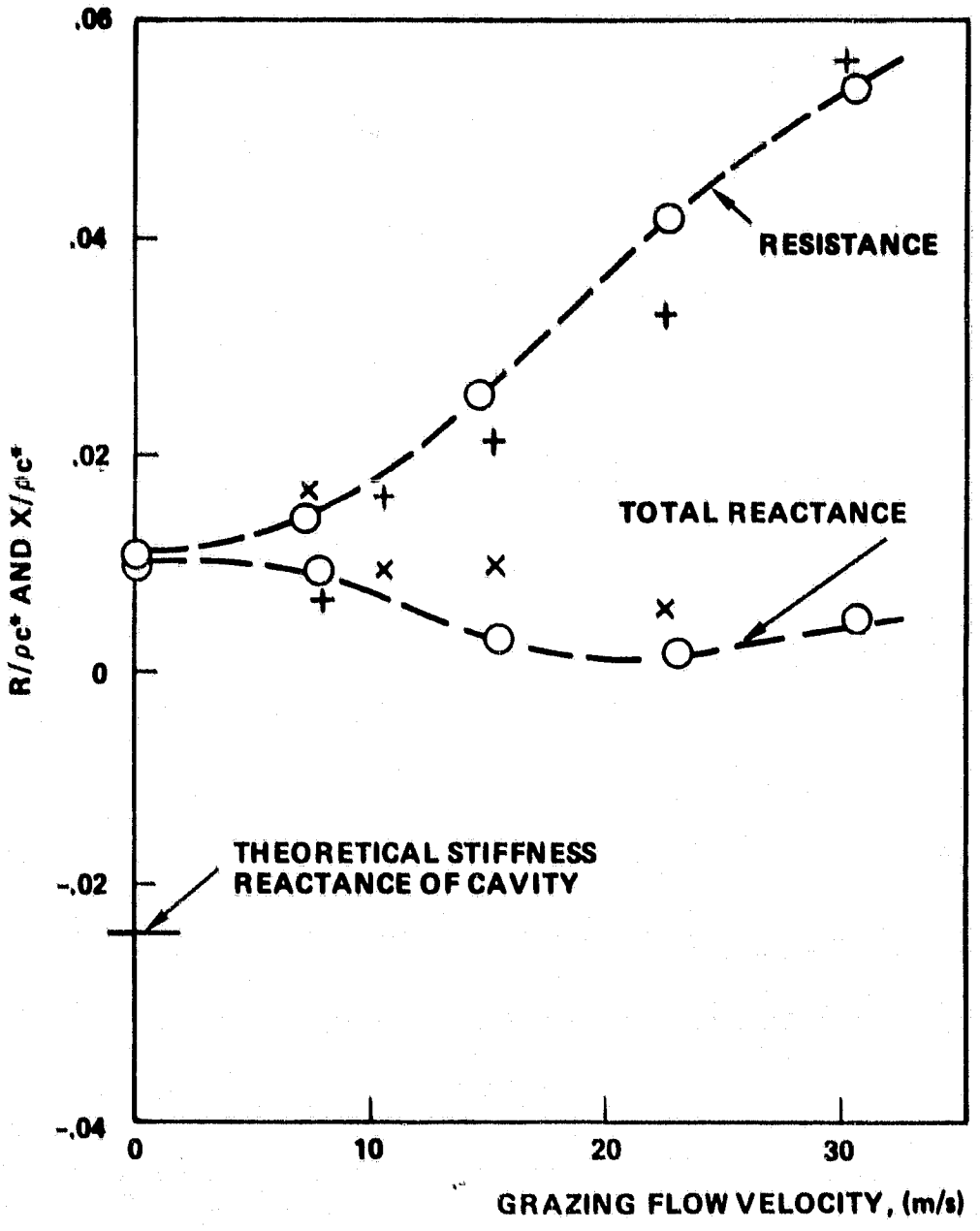

SPECIFIC ACOUSTIC IMPEDANCE
OF THE MODEL (100 Hz, 120 dB)
FROM TWO-MICROPHONES (CIRCLES)
AND MEAN VELOCITY (CROSSES)

of the work of Rice[6]. A modified form of the "lid-model" of Rogers and Hersh [7] is developed, extending the semi-empirical correlation of the resistance to also portray the behavior of the reactance of the resonator.

THE EXPERIMENTAL PROCEDURES

The study was conducted in a wind-tunnel with the model mounted 1 m downstream of the leading edge of a flat plate, spanning the width of the test section (1.2 m). The resonator cavity had a rectangular section 165 mm by 115 mm (streamwise) with adjustable depth. It was contained in an airfoil-shaped strut supporting the mounting plate. The plate had an elliptical nose followed by a strip of porous wall through which suction was applied to thin out the boundary layer. The free height between the mounting plate and the roof of the tunnel was 0.8 m; the flexible roof of the tunnel was adjusted to insure a uniform static pressure over the mounting plane.

The high aspect-ratio slot coupling the resonator cavity to the flow was 6.35 mm deep, 7.62 mm in the streamwise and 155 mm in the crosstream direction. Tests showed that the wave forms of the acoustic velocity were independent of spanwise position except within about half the characteristic slot dimension from the edges (about 5% of its total area).

A 200 watt electrodynamic speaker 0.46 m in diameter was mounted in the roof of the test section directly over the resonator (in a pressure-equalized cavity). A thin plastic membrane was stretched over the speaker to maintain a smooth boundary. The experiments were conducted at a constant excitation frequency of 100 Hz and a fixed power input of 110 watts. The resulting sound pressure level at the resonator orifice varied between 120 and 122 dB (re.20 μ Pa) depending

ORIGINAL PAGE
BLACK AND WHITE PHOTOGRAPH

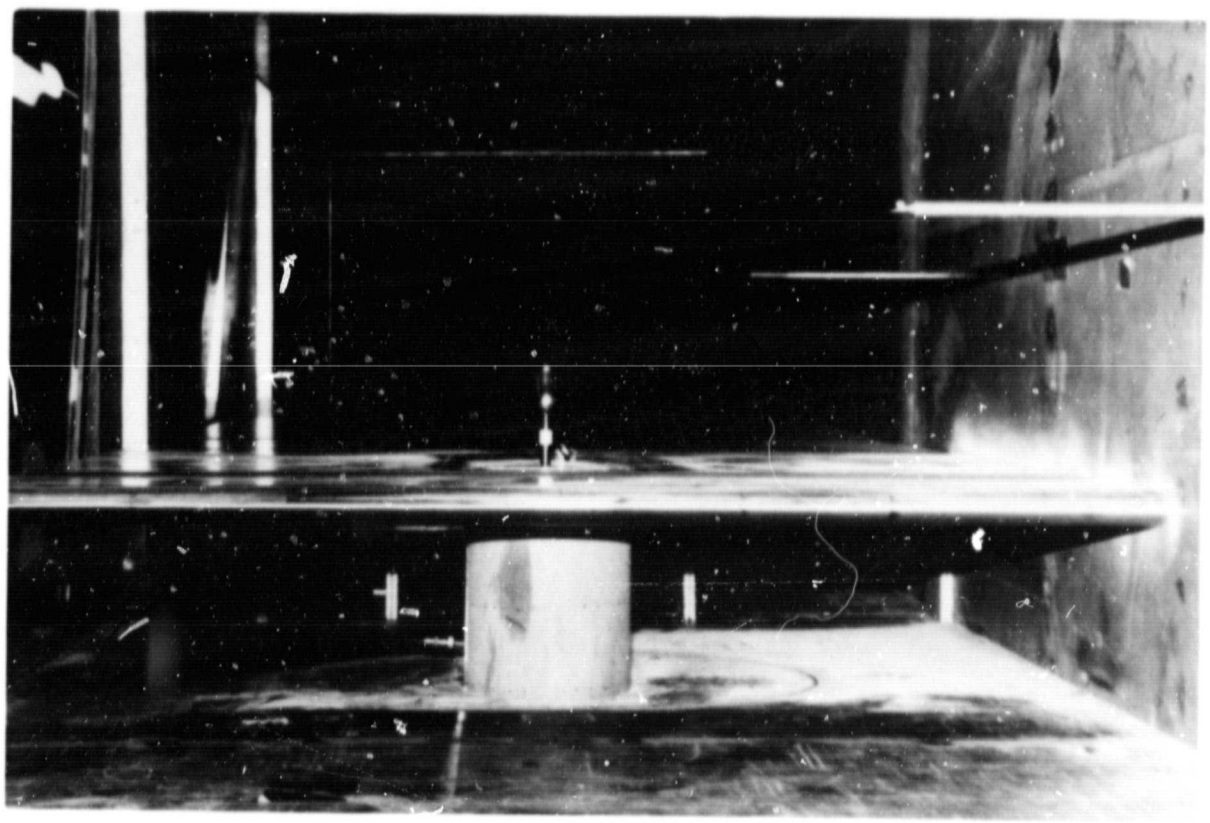

THE MODEL MOUNTED IN THE WIND TUNNEL

on the tunnel velocity. There was no significant distortion in the wave-form of the incident pressure due to reflections and resonances involving the tunnel. The resonator cavity was tuned to maximize the induced velocity at the center of the orifice without grazing flow; this resulted in a cavity volume of 0.0133 m^3.

The velocity of the grazing flow, the principal parameter of these tests, varied between 6.8 and 30 m/sec. The momentum thicknesses of the upstream boundary layer profile varied between 5 and 15 percent of the streamwise length of the slot. The profile followed the one-seventh power law. The noise level in the tunnel at the highest test velocities was measured at 85 db; the free stream turbulence was less than 0.5 percent of the flow velocity.

Pressures were measured in the resonator cavity and on the orifice plate with flush-mounted microphones; each instrument and its individual pre-amplifier was calibrated for attenuation and phase-shift against a common reference. The vector velocities in and the resonator orifice were measured using a Thermal Systems Inc. split-film anemometer, which, because of the central role, will be described in additional detail below. The anemometer reached the slot from downstream. It could survey an area of about 5 x 5 cm in the plane normal to the slot with a resolution of 0.127 mm; its motion was controlled by stepping motors actuating the leadscrews of the traversing mechanism.

The TSI "split-film' probe is a directional hot-film anemometer using two separate sensors deposited each on approximately half the

circumference of a quartz fiber, 0.15 mm in diameter. The sum of the heating currents of both films required to keep them at constant temperature is proportional to the quarter power of the mean velocity, as in ordinary hot-wire anemometry; the difference of the squared currents is approximately proportional to the sine of the angle of the flow relative to the plane of the "split". Using two such probes side by side with the planes of the split oriented at 90 degrees to each other, one can measure the local vector components of two-dimensional velocity fields in four quadrants with a spatial resolution better than 0.15 mm. The relative size of the probe is approximately represented by the dots showing the array of measurement points on figure 10. No other instruments except laser-dopler velocimeters can offer such a resolution; the LDV requires seeding and raises the issue of lag in the motion of the tracers in the unsteady, highly sheared and nonuniform flow over the resonator orifice.

The calibration of the split-film probe is not as simple as that of single-element hot wire. This arises from the thermal coupling of the two half-films by conduction through their common substrate. Instead of using an analytical approximation to its behavior, the probe outputs were reduced to components of the vector velocity by direct comparison with calibration data stored in the memory of a microprocessor. The signals were preprocessed by forming the sum and the log of the ratio of the squared outputs, using precision analogue circuitry; this results in a more uniform distribution of the accuracy of digitalization. Antialiasing filters with a cutoff

frequency of 1250 Hz were used. A look-up table involving 8192 entries of flow velocity and orientation was generated in a special calibration channel. The calibration procedure was carried out using exactly the same signal-acquistion chain as that used to collect data insuring that nonlinearities in the electronic components were accounted for.

The transient response of the split-film probe depends on its orientation, the mean velocity of the flow and the frequency of the disturbance. Figure 2 illustrates the phase-shift of the sum-signal relative to a constant-temperature hot wire. (The amplitude attenuation and the behavior of the difference-signal correlate equally well). The absolute value of the phase shift at the reference condition depends on the circuitry and on the setting of the overheat ratios. In principle, it is possible to reconstitute the input from the measured waveforms by an iterative procedure using such calibration data, but this is not practical. Accordingly, all measurements where corrected for phase-shift and attenuation at the mean operating condition of the run; the uncertainty in the phase information in the following results is estimated at about 5 degrees and 3 percent in the amplitudes.

The difference-signal is sensitive to drift in the relative overheat of the two halves of the split-film. This changes the indicated orientation of the probe to the flow but does not significantly affect its sensitivity. Accordingly, the instrument was periodically returned to a fixed reference point in the free stream

FIGURE 2

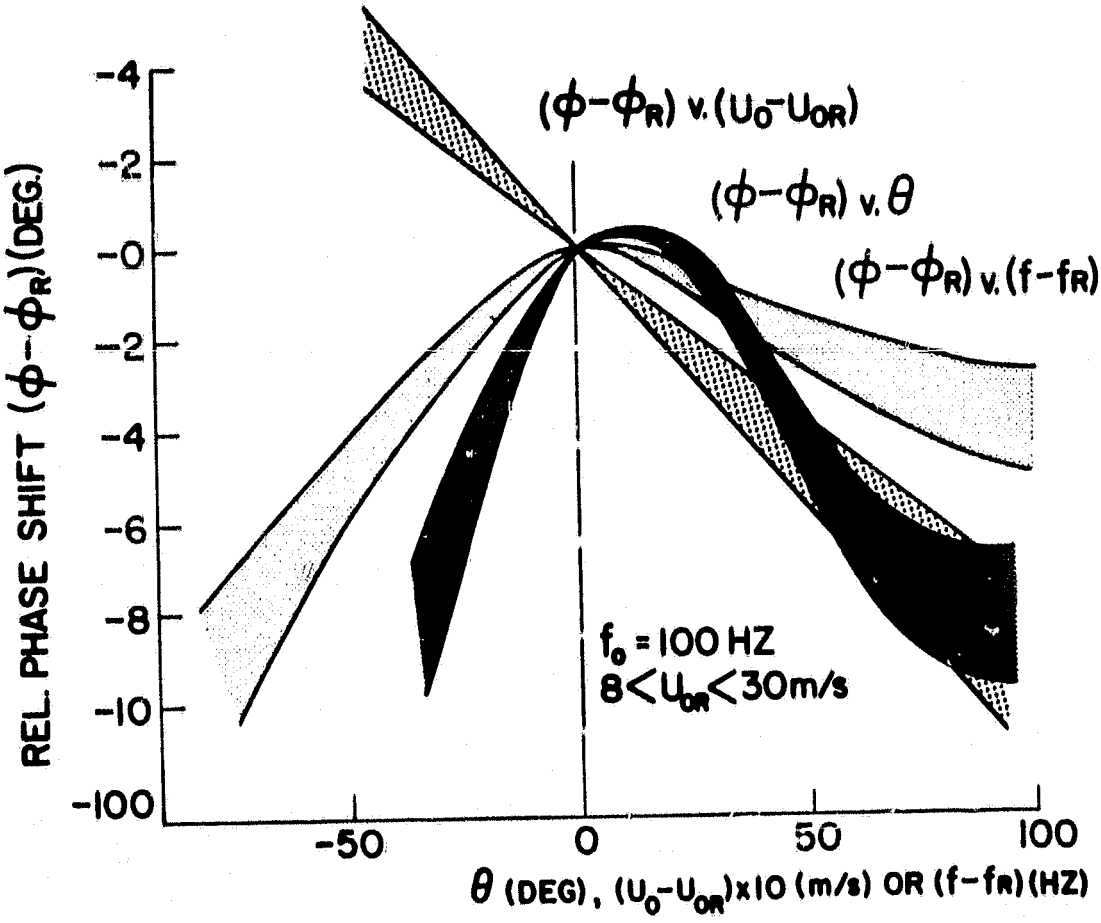

SUM-SIGNAL PHASE SHIFT CALIBRATION

and the appropriate constants in the data reduction program were readjusted. The zero shift correction never exceeded 3 degrees; the procedure is more accurate than rebalancing the anemometer bridges.

The probe was oriented geometrically at 30 degrees to the free stream so that the fluctuating vector velocity remained as much as possible in the two forward quadrants relative to the plane of the split. The minimum distance of approach to the wall was 0.3 mm or 4 percent of the characteristic dimension of the orifice. The distance is measured from the wall to the centerline of the probe.

The question arises as to the accuracy of the probe in highly sheared flow: velocity gradients over a distance of the order of the diameter of the probe can be expected to result in a false indication of orientation. To gain some insight into this problem, the probe was used to traverse the wake immediately downstream of a symmetrical airfoil, at several stations spaced 0.25 mm apart. The measured streamwise velocity and its streamwise gradient were calculated. The two-dimensional mass-conservation equations were then integrated to yield the local cross-velocity. This was compared to the cross velocity indicated by the probe. The results for a traverse close to the trailing edge of the airfoil are shown on figure 3. The streamwise velocity gradient in the wake at this station is about 10^4 inverse seconds; it is comparable to the highest mean shear encountered above the test orifice. The internal consistency of this test is clearly encouraging; at stations further downsteam in the wake a progressively better accord was obtained.

FIGURE 3

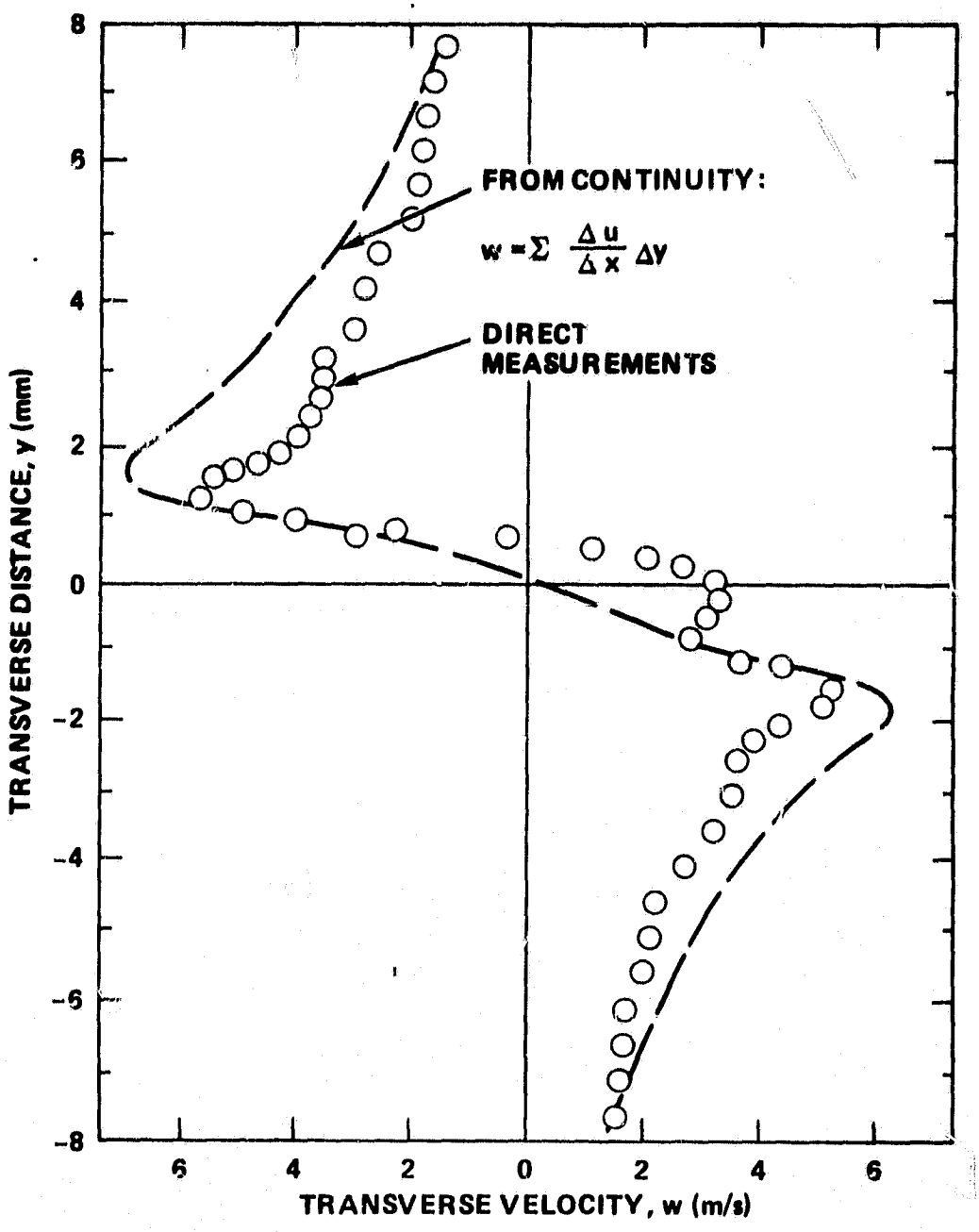

TRANSVERSE VELOCITY PROFILE AT x = .51 mm DOWNSTREAM OF THE TRAILING EDGE OF AN AIRFOIL

The entire data-acquisition procedure was controlled by the microprocessor. It generated the acoustic excitation as a 64-segment approximation to a harmonic function. The data were sampled during each of the 64 phase intervals over 4000 cycles, sorted, averaged, reduced and stored on magnetic discs in real time. Cavity and tunnel reference pressures were acquired once every 5 cycles. After completing the measurements at 75 positions of the probe it was automatically returned to the free stream reference location for recalibration against drift. A survey of the flow over the orifice at one grazing velocity required 15 hours of continous testing.

An overall evaluation of the accuracy of the present results is obtained by intergrating the normal velocity component along the wall and the orifice for a full cycle. If the angle of the flow at the reference station (one orifice length upstream and two lengths above the wall) is set to zero, we find a small mean inward flux into the wall; alternately, if the net inflow is set to zero, the flow at the reference station is found to diverge by 3 to 6 degrees. This can be partly explained by a displacement effect of the boundary layer. Indeed, vector-velocity profiles measured up and downstream of the orifice yield a rate of growth of the boundary layer which corresponds to between 3^{o} (at 7.6 m/s) and 0.5^{o} (at 22 m/s) outward deflection of the free stream.

RESULTS

Velocity waveforms

Figure 4 shows examples of the primary data, the instantaneous streamwise and crosstream velocity at various distances above the plane of the orifice, at 25% if its span (fig 4a), the downstream corner (fig 4b) and along the wall downstream of the orifice (fig 4c). The velocities are reference to the maximum volume-velocity calculated from the derivative of the pressure in the cavity. The streamwise velocity is plotted relative to its local average. The more complete set of such data is complied in a separate report [8].

It is difficult to interpret these results. The individual waveforms are increasingly distorted towards the wall the downstream corner of the orifice. In spite of this waveform of the space-averaged crossvelocity along the plane immediately above the orifice i.e.: the variation of the volume flow into the orifice (not shown) is remarkably sinusoidal. This checks the relatively harmonic variation of the pressure in the cavity of which examples are shown on figure 12. A general characteristic of the waves, particularily noticeable at higher grazing velocities, is that the inflow phase seems to last somewhat longer than half the cycle while the outflow is compressed in time. The largest perturbations occur near the downstream corner of the orifice. Note the reversal in the phase of the streamwise

FIGURE 4a

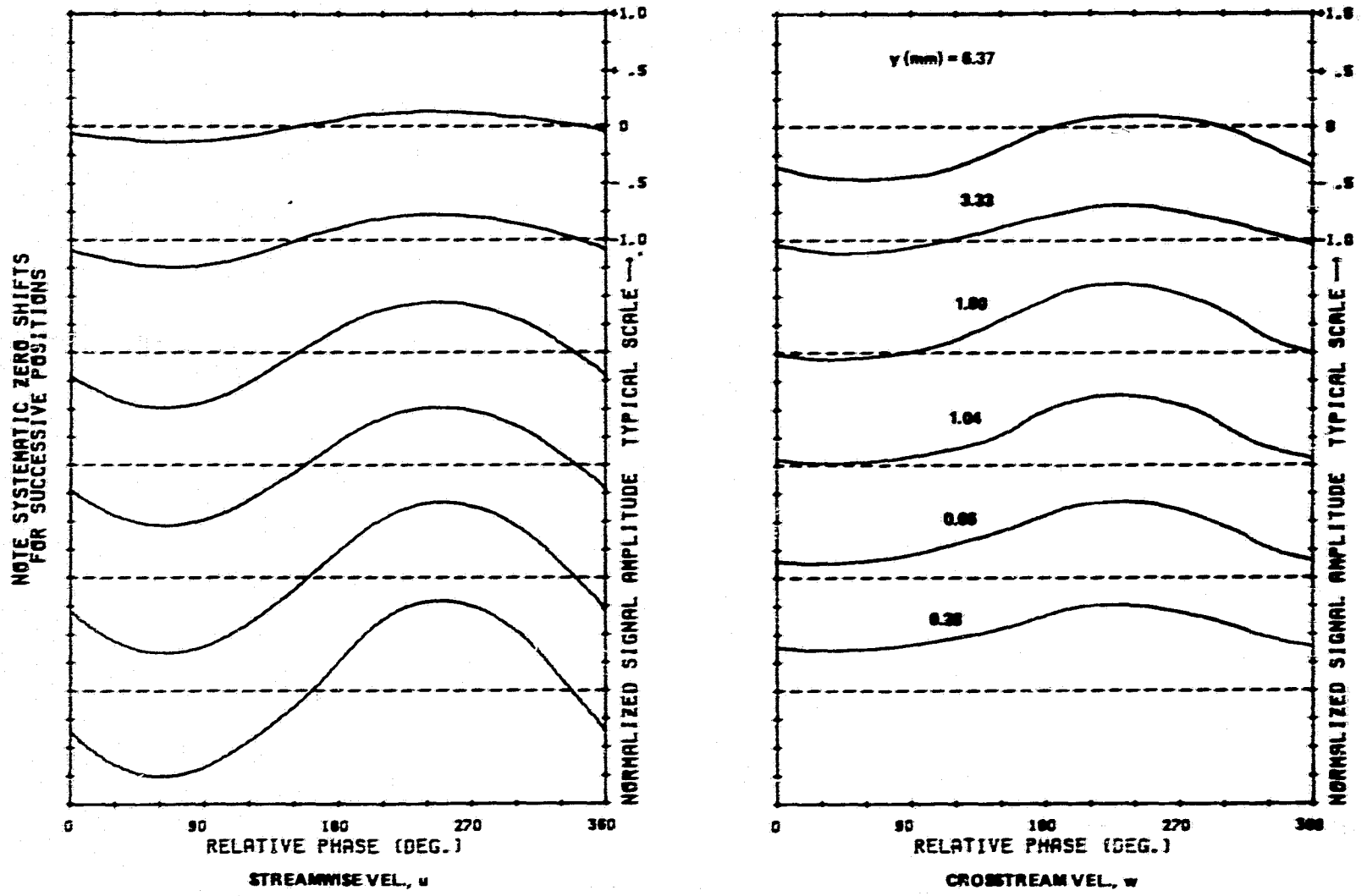

VARIATION OF THE PERTURBATION VELOCITIES WITH DISTANCE FROM THE WALL AT $\frac{x}{s} = .25$ $U_\infty = 22.86$ m/s

FIGURE 4b

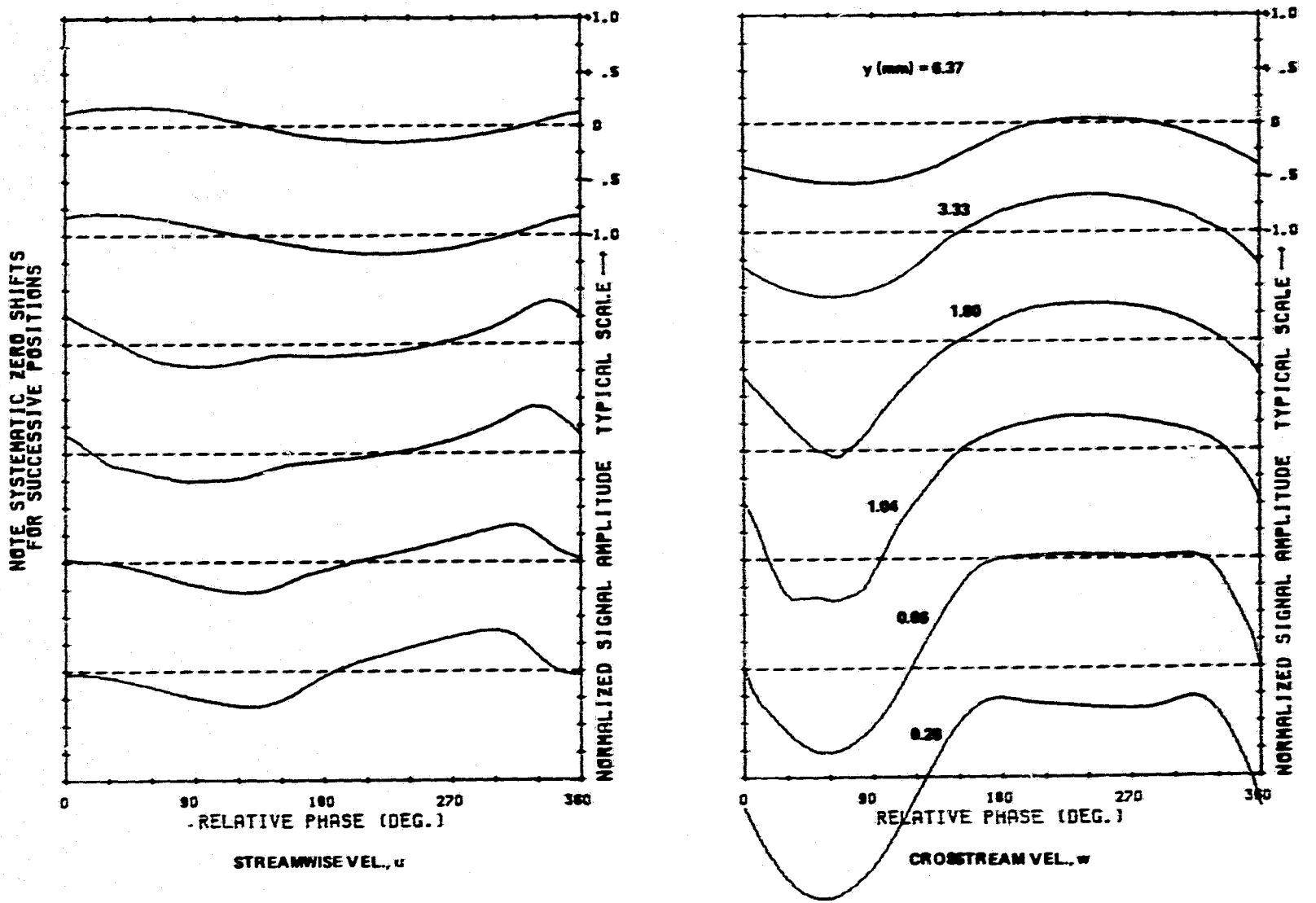

VARIATION OF THE PERTURBATION VELOCITIES WITH DISTANCE FROM THE WALL AT $\frac{x}{s} = 1.0$ $U_\infty = 22.86$ m/s

FIGURE 4c

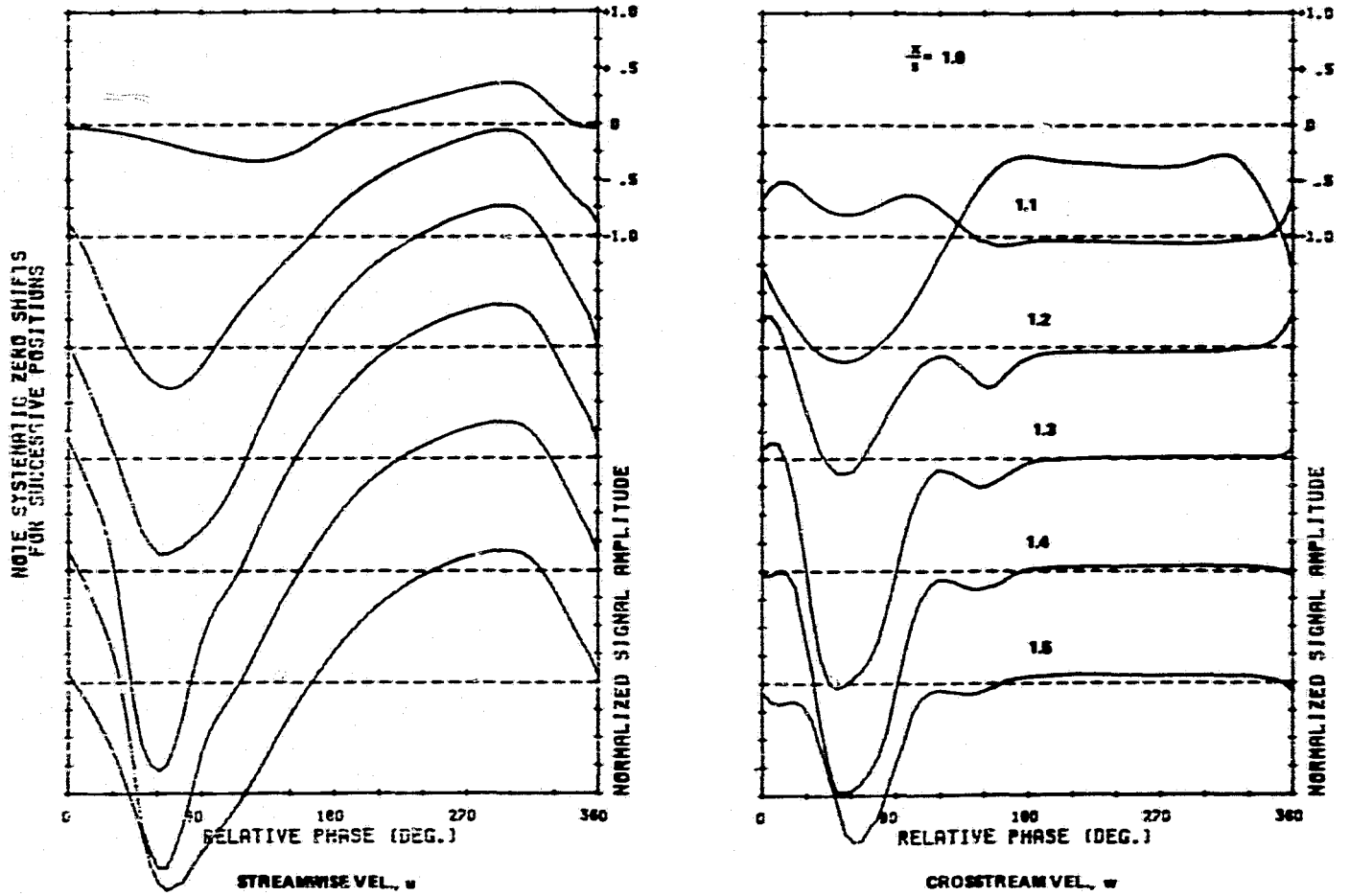

VARIATION OF THE PERTURBATION VELOCITIES DOWNSTR. OF THE ORFICE

AT $\frac{Y}{s}$ = .04 (0.28 mm ABOVE WALL); U_∞ = 22.86 m/s

velocity at about 2mm from the wall at this velocity of the grazing flow (this does not happen at low grazing speeds).

Typical plots of the phase and amplitude of the first harmonic of these waves are shown on figure 5. For the ideal case of a simple line source, the streamwise velocity along the normal velocity across a plane parallel to the wall vary as the inverse of (x^2+1) and $(x+1/x)$, respectively. The phase of the former changes discontinuously by π at the centerline and that of the latter is constant. In the general sense, these features are present in figure 5. As the grazing velocity increases, the axis of the perturbation field is swept downstream. Also, its spread is decreased. It appears as if only the downstream portion of the orifice were "open" at higher grazing velocities; the effective characteristic dimension of the orifice is decreased.

Figure 6 shows the gradual decay of the distortions in the amplitude of the normal velocity with distance from the wall. Pronounced irregularities in a w and its phase appear immediately downstream of the reattachment corner indicating a local separation and flow reversal. Figures 5 and 6 show local peaks, the interpretation of which is difficult. However, they appear to be real: Their evolution from one station to another can be followed with remarkable consistency on the more complete set of these results.

FIGURE 5

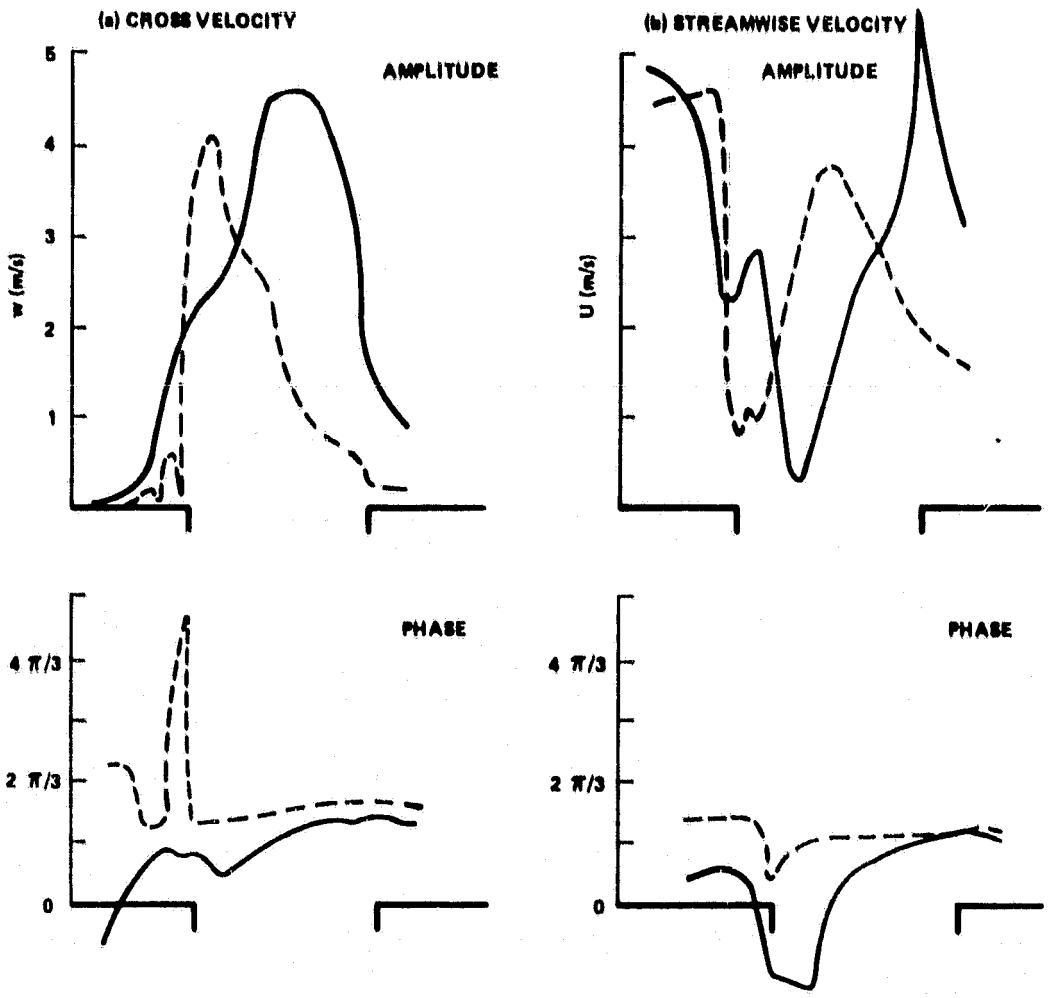

FIRST HARMONIC OF THE PERTURBATIONS AT $y/\delta = .04$
GRAZING VELOCITY: - - - 23 m/s, —— 7.6 m/s

FIGURE 6

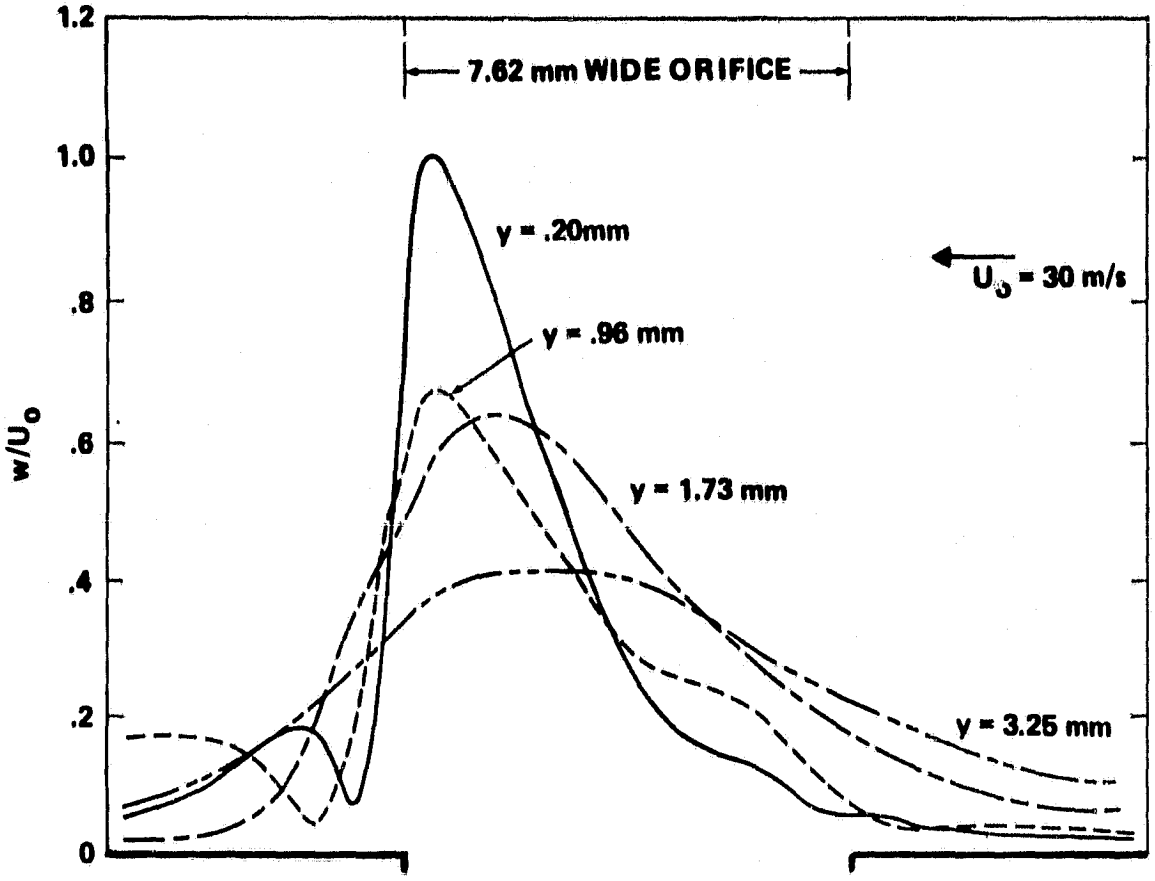

MAGNITUDE OF THE FUNDAMENTAL HARMONIC NORMAL VELOCITY, w

DECAY OF THE CROSSTREAM PERTURBATION AWAY FROM THE WALL

The perturbation field

The overall structure of the field emerges from figure 7 which shows the local perturbation velocity vectors above the orifice at various phases. The phase is measured relative to the volume-velocity (calculated from the derivative of the cavity pressure).

The flow pattern clearly evokes a pulsating source and an unsteady vortex located at a small distance above the wall downstream of the orifice. The strength of the vortex pulsates coherently with that of the source. The wall implies the existance of an image-vortex below the wall such that the sum of the normal velocities induced by the pair at the wall is zero.

The physical interpretation of the pulsating source is obvious; Rice [6] analyzed such a model. However, he did not include the pulsating vortex which portrays the contribution of the external flow to the perturbation field. The flow separation vortex at the edge of the jet out of the orifice during outflow is intuitively clear; it is observed and discussed in ref 4, in the absence of grazing flow. The opposite circulation during inflow is less obvious. It occurs due to the interaction of the grazing flow with the orifice. Consider the time-average perturbation relative to the upstream undisturbed flow, i.e., the mean vector velocities at each grid-point subtracted from the velocity upstream of the orifice at the same distance from the wall. The resulting field is shown on figure 8. It indeed shows a steady circulation pattern (which is emphasized) which would not exist but for the disturbance due to the orifice.

FIGURE 7(a)

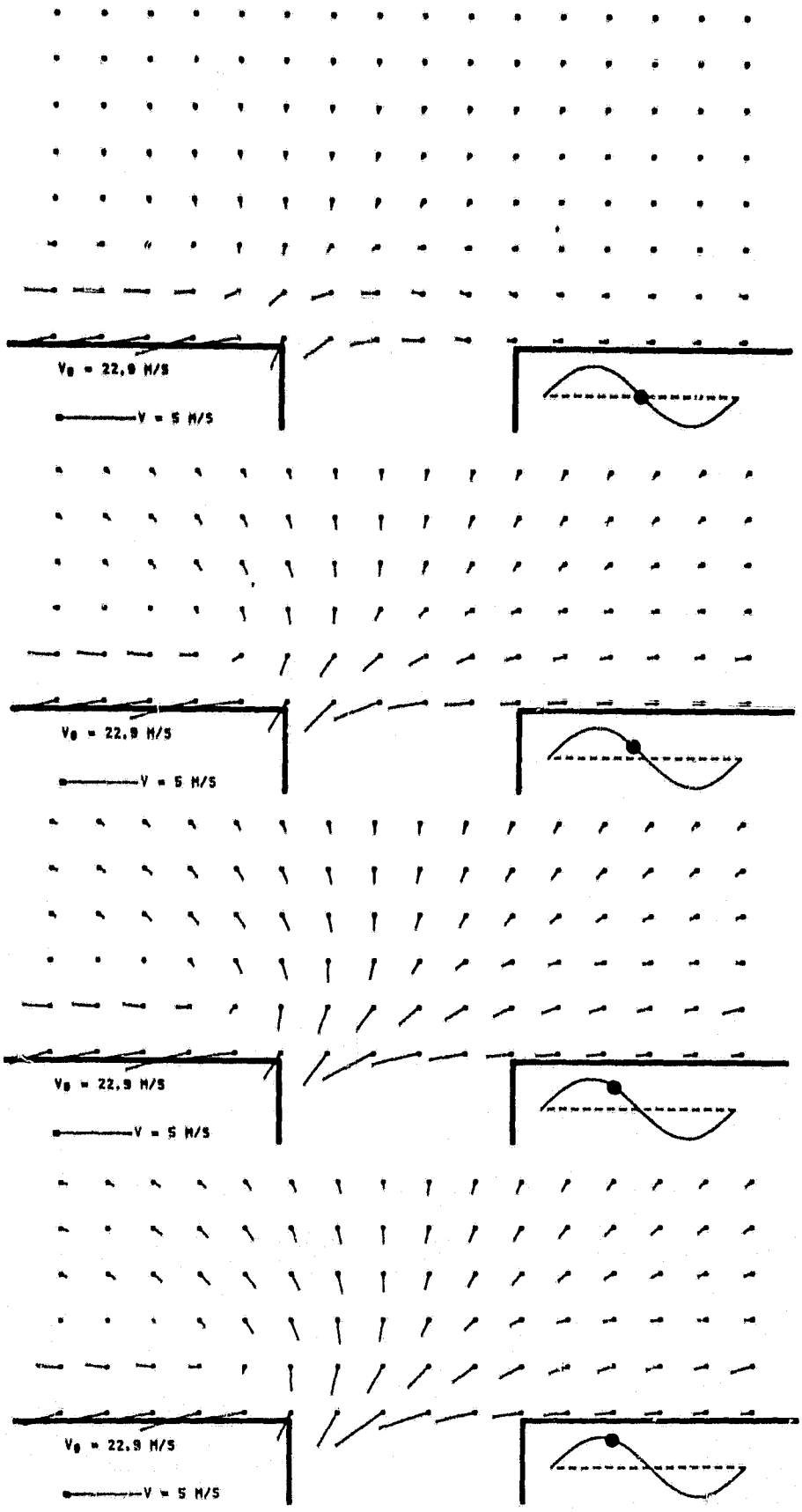

VECTOR PERTURBATION FIELD AT U_0 = 22.9 m/s (RIGHT TO LEFT)

FIGURE 7(b)

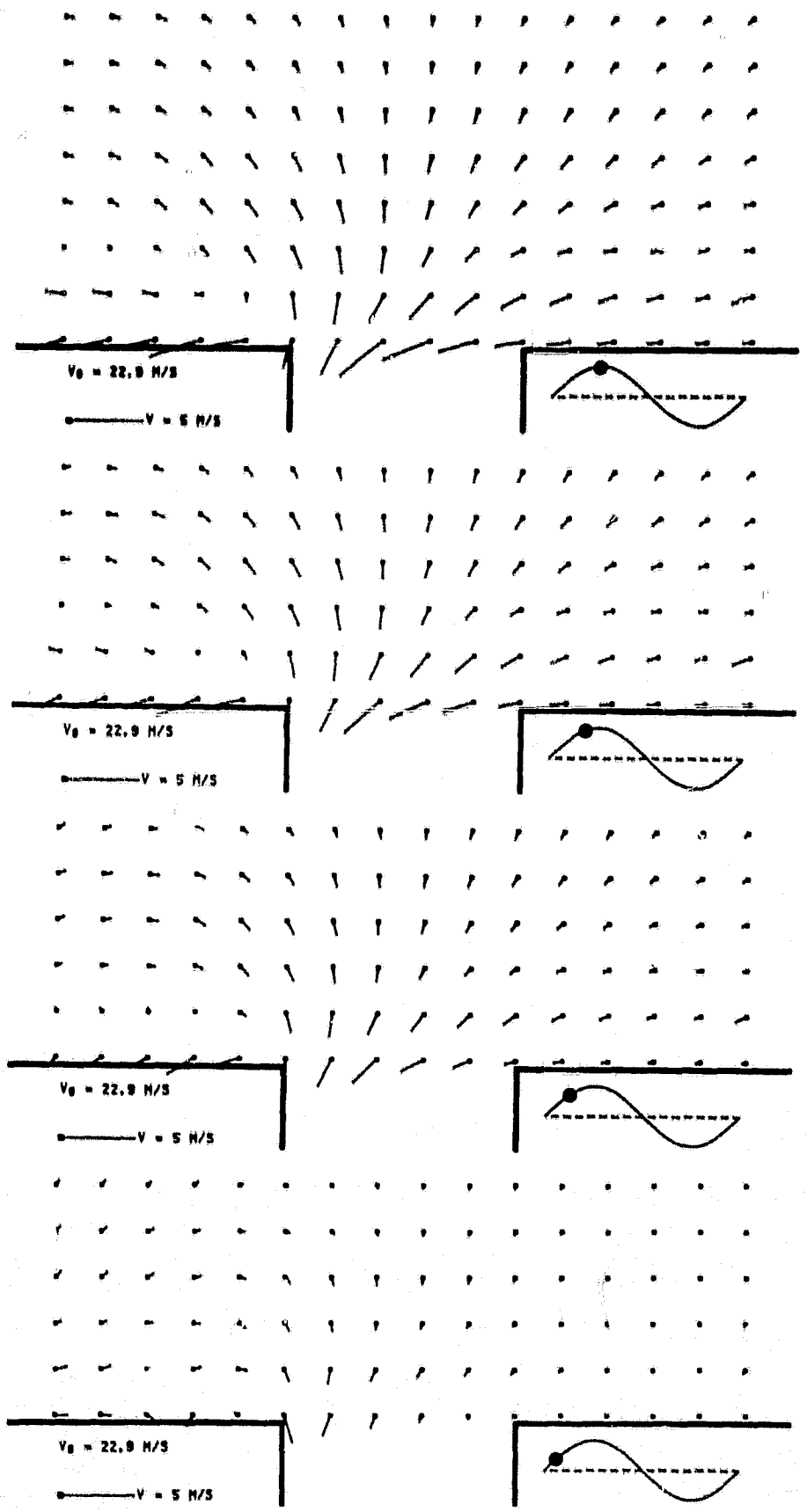

VECTOR PERTURBATION FIELD AT U_0 = 22.9 m/s (RIGHT TO LEFT)

FIGURE 7(c)

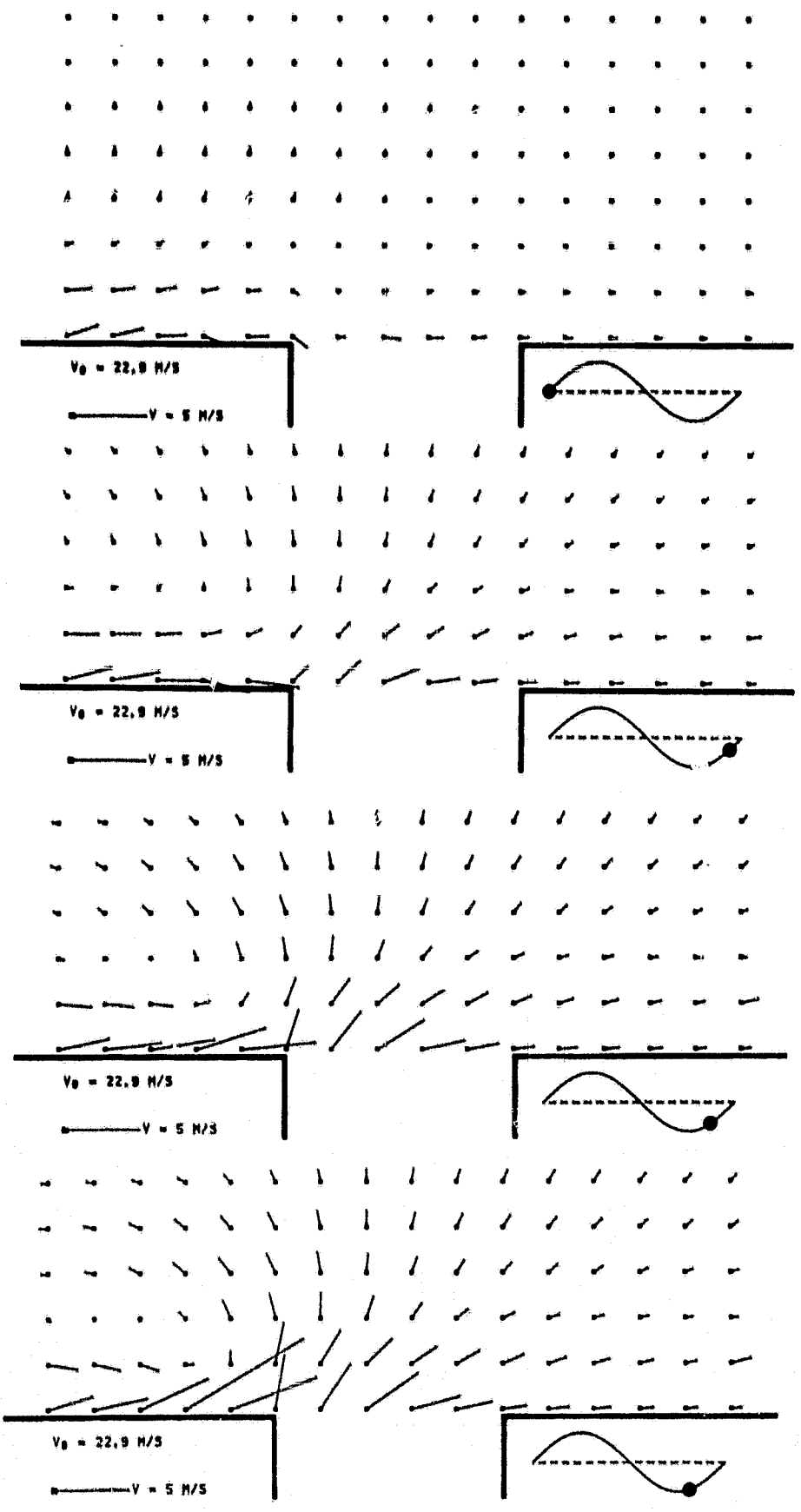

VECTOR PERTURBATION FIELD AT U_0 = 22.9 m/s (RIGHT TO LEFT)

FIGURE 7(d)

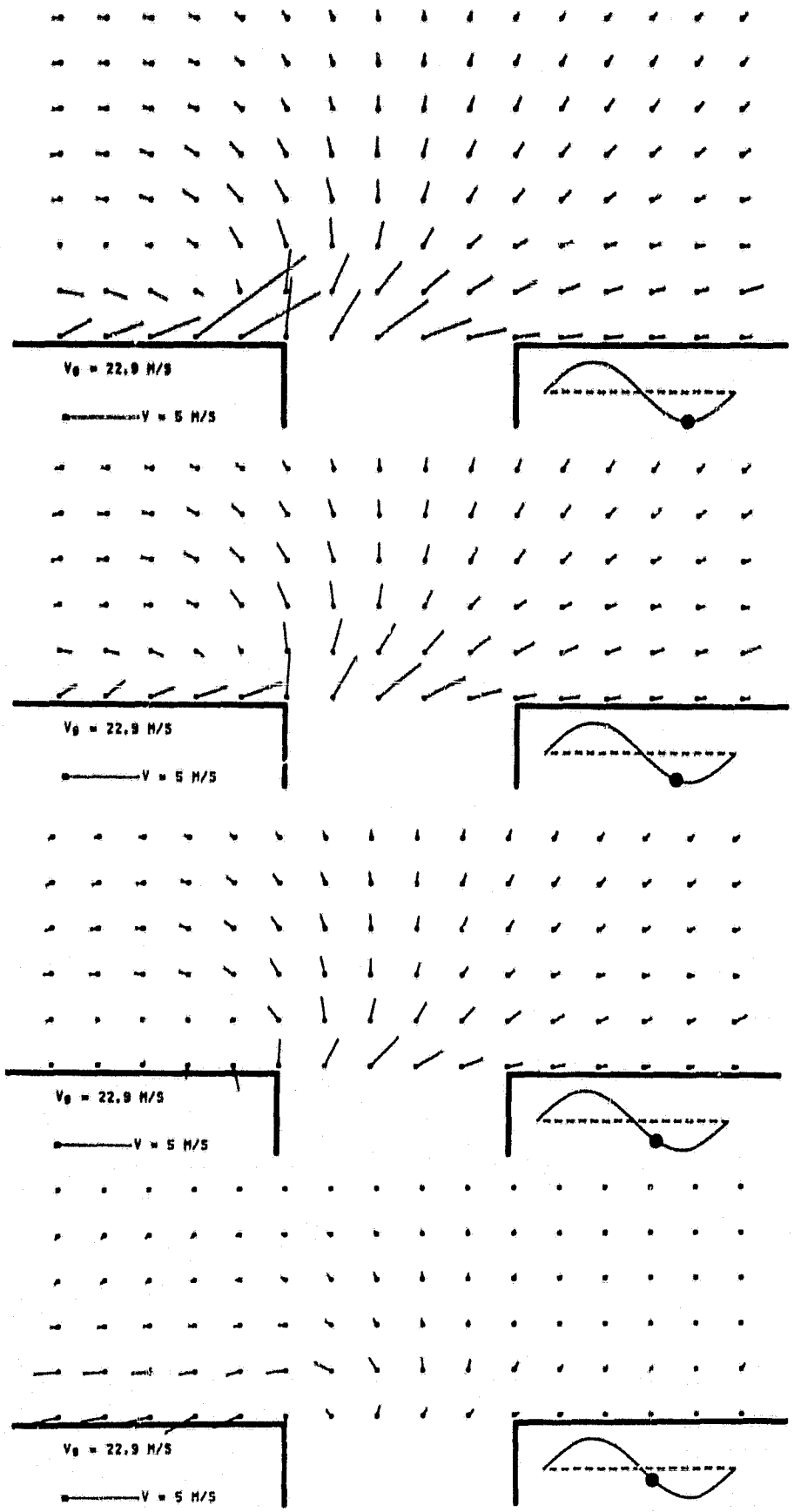

VECTOR PERTURBATION FIELD AT U_0 = 22.9 m/s (RIGHT TO LEFT)

FIGURE 7(e)

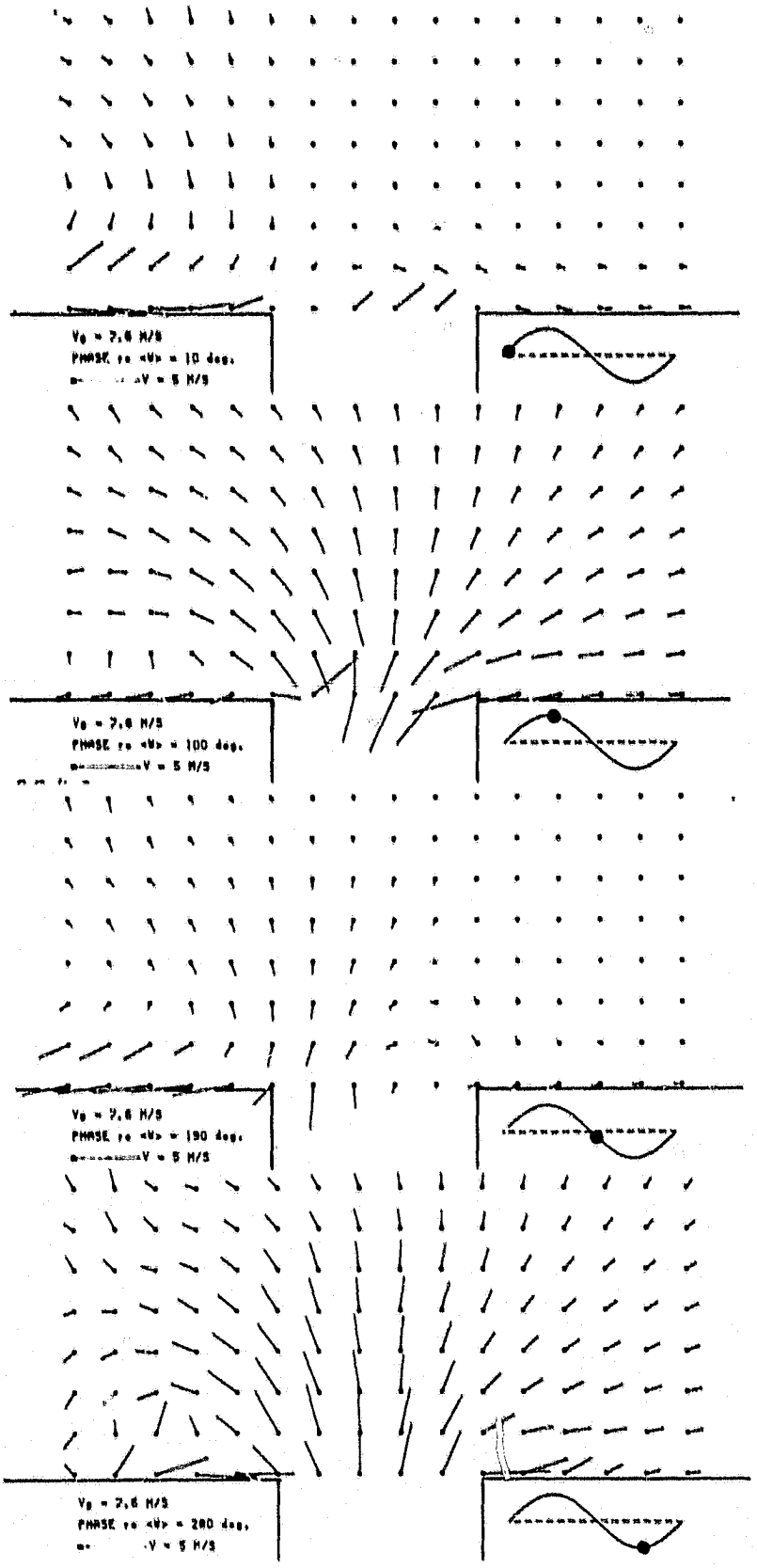

VECTOR PERTURBATION FIELD AT 7.6 m/s (RIGHT TO LEFT)

FIGURE 8

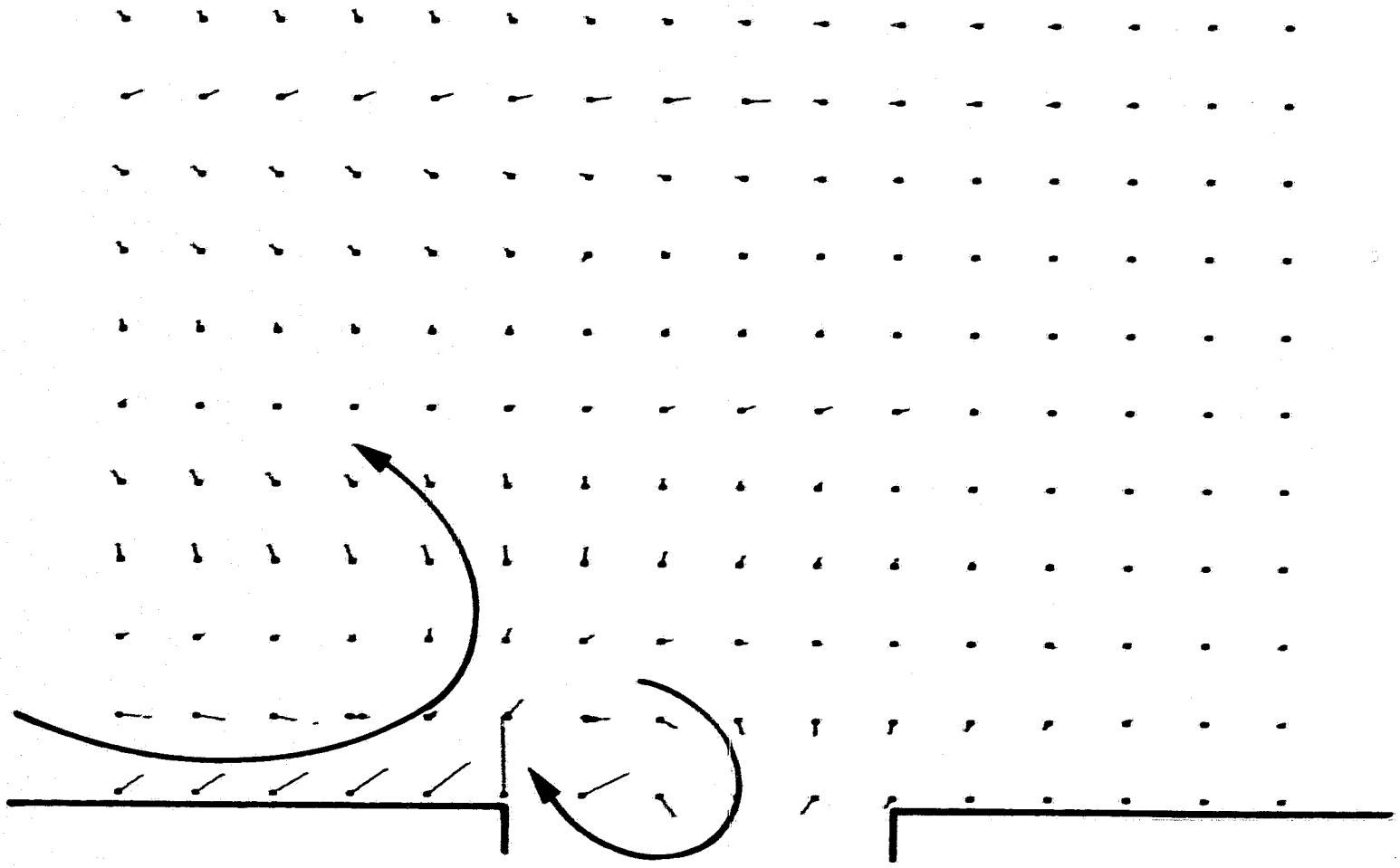

TIME-AVERAGED PERTURBATION FIELD (REL. TO UPSTREAM B. L. PROFILE)
U_o = 22.9 m/s (RIGHT TO LEFT)

The character of the perturbation field does not change with the grazing velocity. The magnitude of the perturbation at equivalent points in the cycle is, in general, larger at lower grazing velocities. The phase of the source relative to that of the vortex and to the phase of the volume-flow into the cavity appear to depend on the velocity of the grazing flow. One can easily identify two phase-references directly from these data. The first is the instant at which the bulk of the perturbation field (say, in the upstream quadrant) becomes stationary, such as the situation depicted on figure 7. It occurs at approximately 22^{o} and 10^{o} after the zero-crossing of the volume flow for 22.9 and 7.6 m/s, respectively. The second is the instant at which the streamwise velocity along the wall downstream of the orifice is zero. This happens at about 10^{o} and 50^{o} for these grazing velocities.

While this cannot be determined precisely, we are of the impression that the effective location of the vortex moves closer to the wall and to the source at lower grazing velocities. (This could imply that, as the grazing velocity tends to zero, the vortex and its image coincide with the source and cancel.)

A source-vortex model

Only so much can be said from inspection of data without an analytical model. An attempt to formulate one is in progress. The kinematics of the the instantaneoous perturbation field, treated as a quasi-steady problem, is easily written down. It involves five parameter: The strength of the source, the strength of the vortex, two

coordinates of the radius-vector defining their relative location and their relative phase. The data suggest two relationships between them. The streamwise distance between the source and the vortex represents in the first approximation the length of the orifice (it may also depend on the magnitude of the grazing velocity). The streamwise perturbation induced by the source at the location of the vortex must cancel that induced by the image-vortex, i.e., their strengths are related via the size of the orifice. The cross-stream velocity induced by the source at the vortex will cause it to move perpendicularly to the wall. One is lead to prescribe a minimum distance of approach which in the first approximation is zero (vortex doublet) this provides a second condition. Three additional constraints are required to complete the coupling of this perturbation field with the environment. One of these is clearly derived from the relationship between the strength of the pulsating source and the resonator cavity. Another may be sought in the balance between the net streamwise momentum flux induced by this system of singularities and the drag experienced by the grazing flow over the orifice, a parameter which will have to be provided empirically. For example data on the increase in the momentum thickness of the boundary layer from traverses upstream and downstream of the cavity, figure 9. The third condition is not clear at this time; perhaps it can be found from considerations of the energy balance coupling the model to the acoustic excitation.

A Picture of the near-field

A different picture of the flow into the cavity is obtained by

FIGURE 9

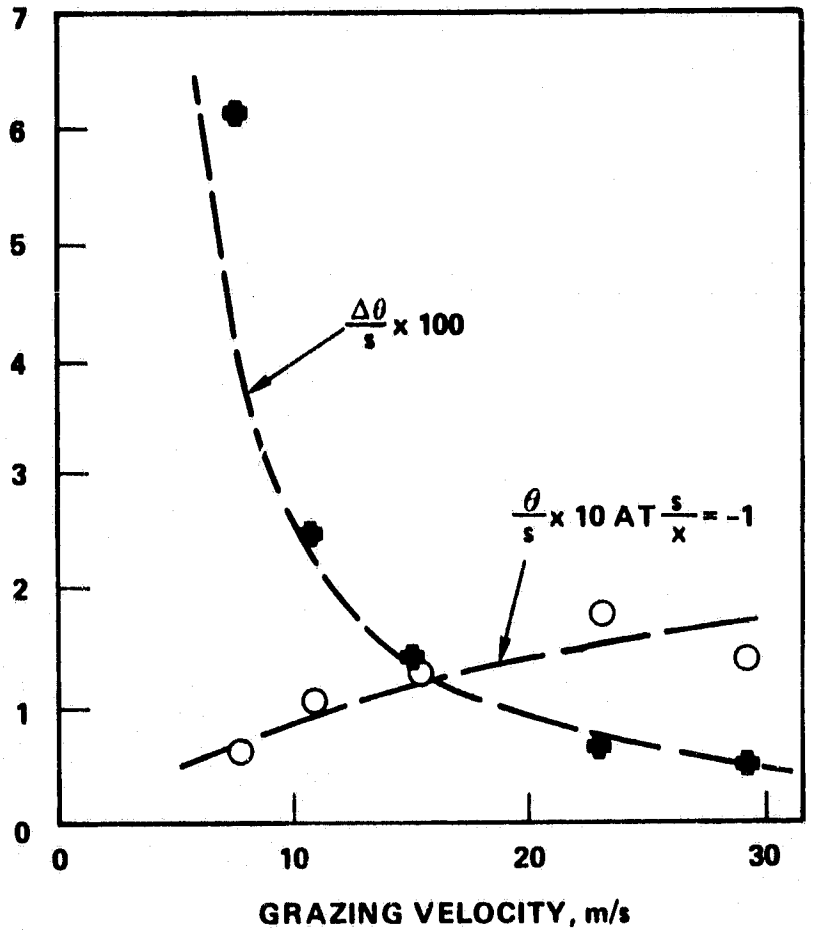

INCREASE IN THE MOMENTUM THICKNESS OF THE BOUNDARY LAYER ACROSS THE SLOT (x/s - 1.0 TO x/s = +2.0)

plotting the trajectories of imaginary tracers injected into the flow from upstream and along the surface of the slot at a given instant. Their motion through the grid of data points is calculated; the numerical code and an evaluation of its accuracy are described in reference [8]. Figure 10 shows examples of these trajectories; selected fronts of equal time-of arrival are also shown.

At the lower grazing velocity, figure 10a, the flow looks like a regular periodic plume issuing out of the full opening of the slot. At the higher velocity, figure 10b, the plume does not just bend more sharply with the flow, but the upstream portion of the slot appears not to participate in the exchange of mass with the cavity. These patterns are similar to the water-channel flow-visualization pictures provided by Baumister and Rice [2].

Measurements inside the passage are shown on figure 11 in the form of local (total) velocity vectors. This example depicts an intermediate grazing velocity of 15 m/s. Only the "mature" inflow and outflow are shown. The full sequence of these results [8] is interesting in that it shows how the circulating flow along the upstream wall of the passage "unravels" during transitions between inflow and outflow. Traces depicting the flow pattern which have been added for emphasis have no analytical significance.

The channeling of the flow through the passage becomes more pronounced as the grazing velocity increases. Associated with it there is an increasing nonuniformity in the pressure across the slot.

FIGURE 10(a)

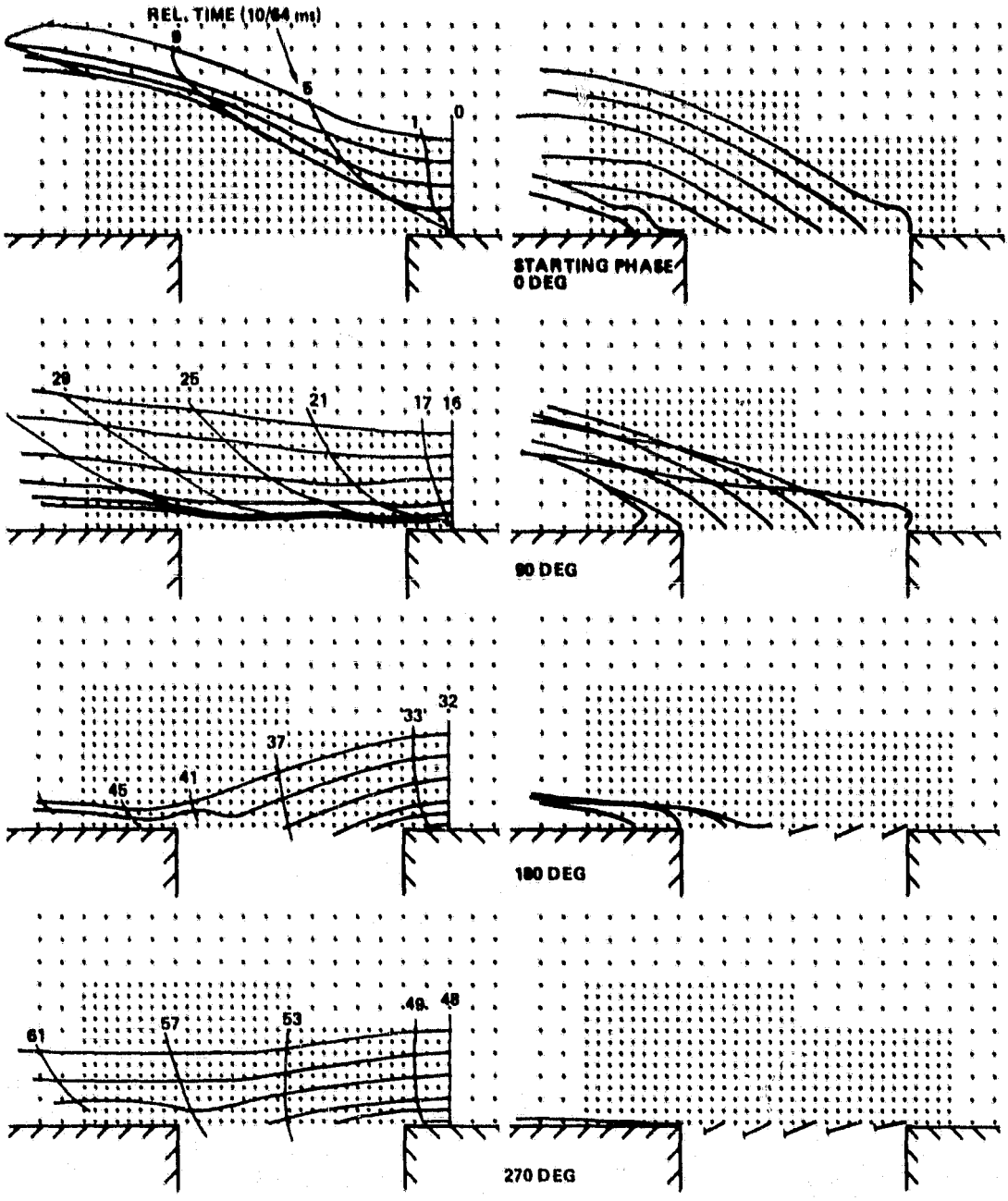

TRAJECTORIES INITIATED AT DIFFERENT PHASES
FROM UPSTREAM (LEFT) AND CAVITY (RIGHT)
U_0 = 7.6 m/s

FIGURE 10(b)

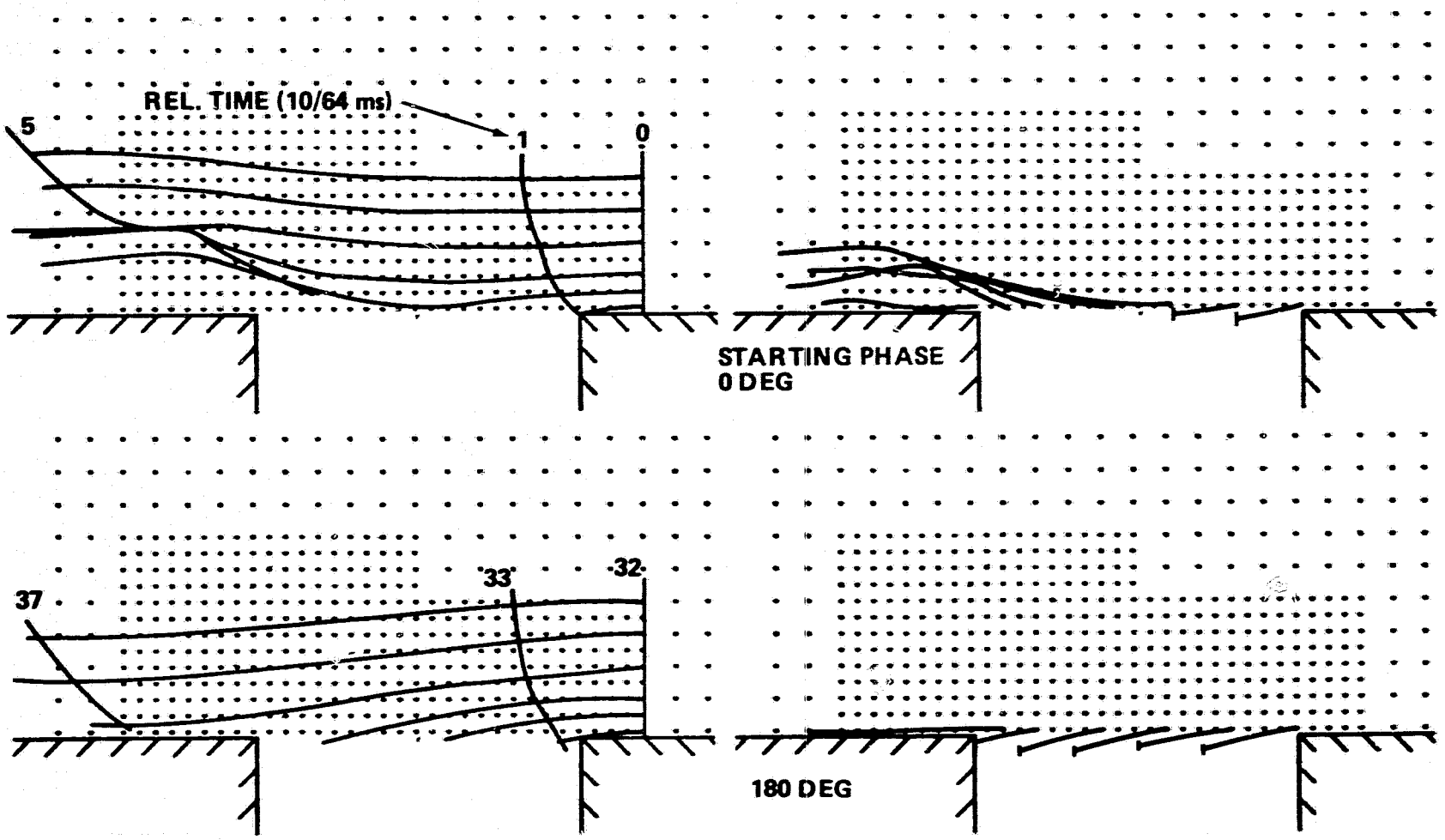

TRAJECTORIES INITIATED AT DIFFERENT PHASES
FROM UPSTREAM (LEFT) AND CAVITY (RIGHT)
U_o = 22.86 m/s

FIGURE 11

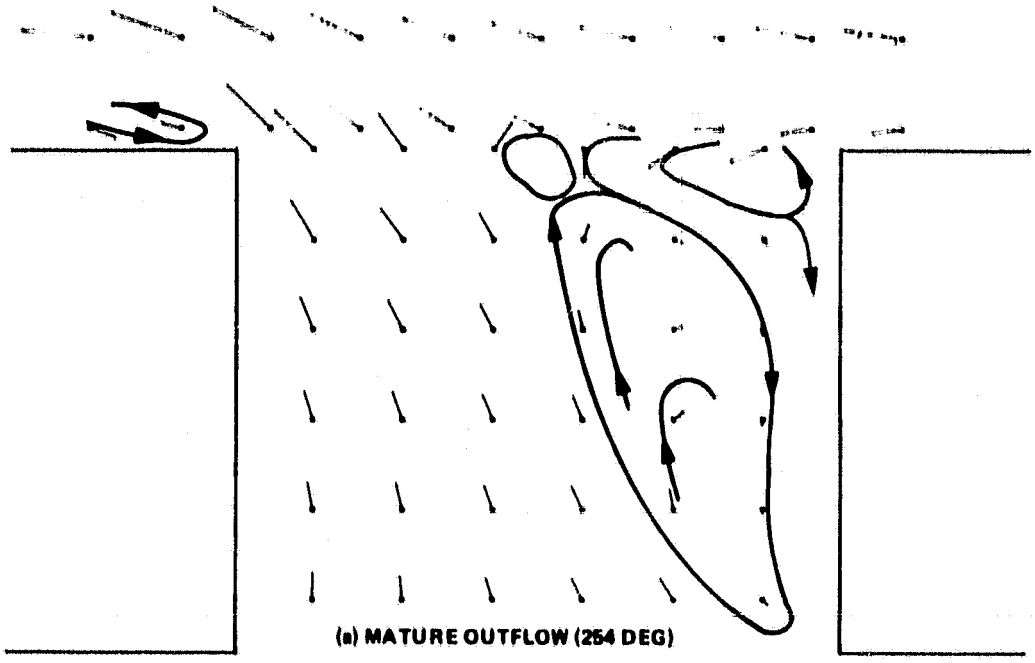

(a) MATURE OUTFLOW (254 DEG)

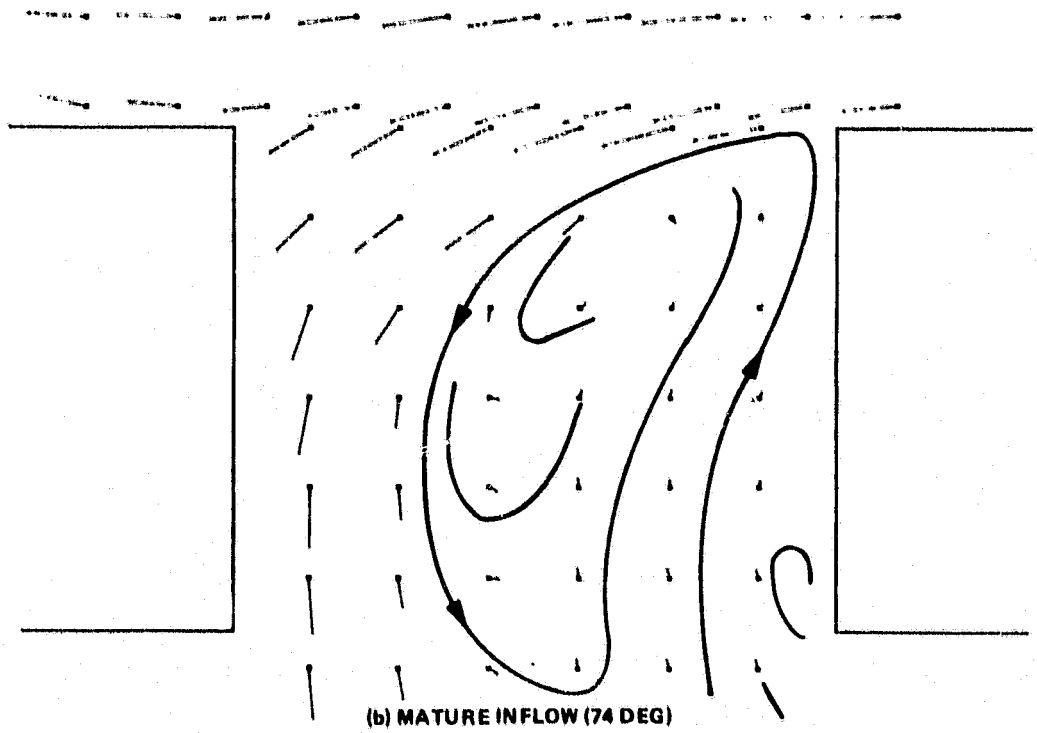

(b) MATURE INFLOW (74 DEG)

FLOW PATTERNS IN THE SLOT AT Uo = 15 m/s

Measurements were made through pressure taps drilled in the side of the slot, 1 mm below the corner using a capacitive pressure transducer mounted in a small cavity in the orifice plate. This special insert was reversible so that the pressures on both the upstream and downstream face were obtained with the same equipment and the attenuation due to the measuring cavity, if any, are balanced out. The data, including the pressure variation in the cavity are plotted on figure 12.

Without grazing flow, the instantaneous pressure is uniform across the orifice and its variation in time is approximately symmetrical with respect to that of the pressure in the cavity. It fluctuates relative to its mean much less than the pressure in the cavity. Local minima (low pressure) occur at about the zero crossings of the cavity pressure; these correspond to a maximum velocity through the orifice and thus appear to be associated with the dynamic pressure drop of the pulsating flow through the orifice.

With grazing flow, the pressure on the downstream face increases significantly relative to that on the upstream face during inflow and falls significantly below it during outflow, indicating sharp centrifugal gradients associated with the turning of the jet around the downstream corner. The peak gradients lag the cavity pressure by about 30 degrees, i.e., the maximum velocity in the opening is no longer in phase with the average velocity (volume-flow) into the cavity.

The structure of the flow in the orifice indicated by these data, which is finer and more precise but basically similar to the flow-

FIGURE 12

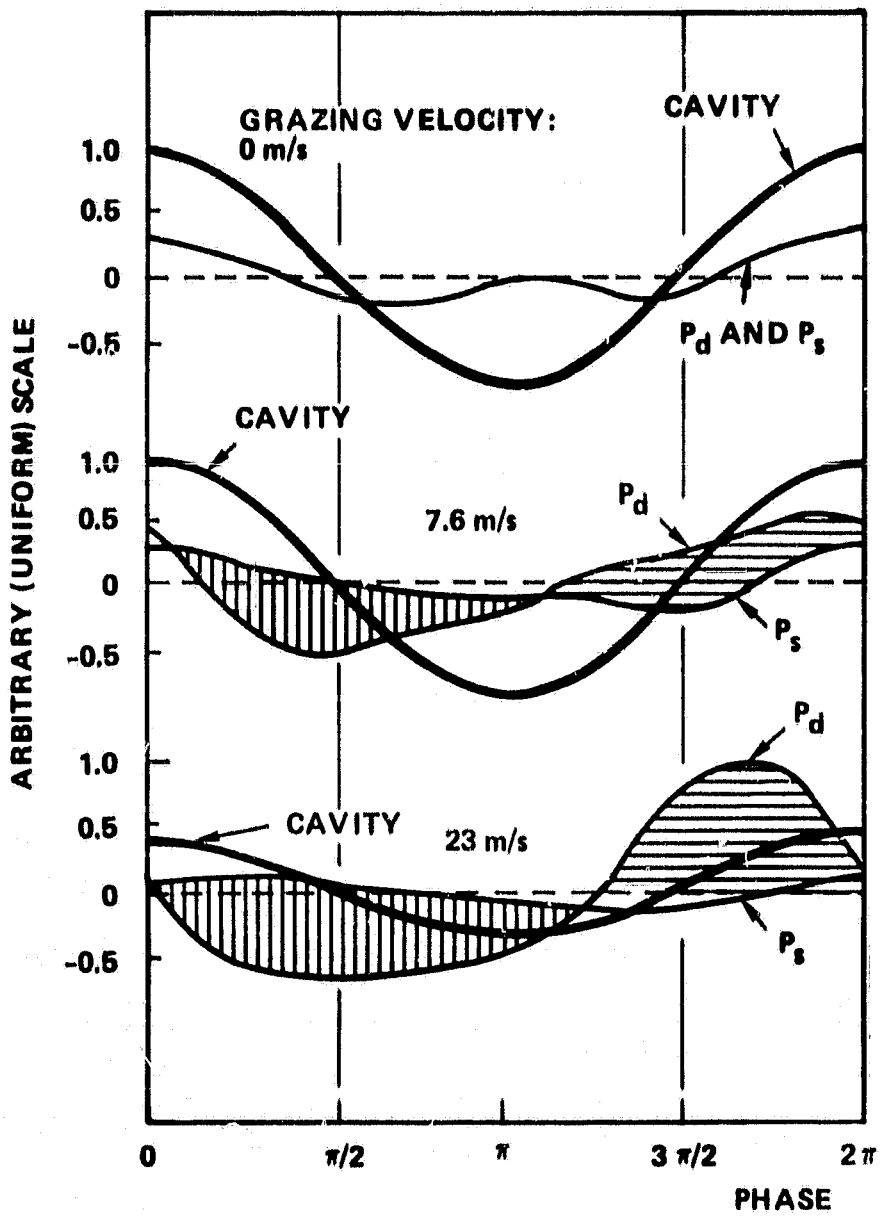

VARIATION OF THE PRESSURE ACROSS THE SLOT
P_d: DOWNSTREAM WALL; P_s: UPSTREAM WALL

visualization results of reference 3. constitutes the conceptual basis of the "lid-model" proposed by Rogers and Hersh[7]. That model and also Rice's[6] solution ultimately relate the problem to an orifice discharge coefficient which is supplied separately from a correlation of steady-state data. It is always possible to define an orifice coefficient heuristically. It does not seem likely to us, however, that the resistance of the orifice controls the structure of the flow. It seems more likely that it is determined by the mechanism of interaction between the two perpendicular streams during outflow.

The "Hinged-Lid" Model

The following model is similar to that in the referenced analysis with the essential difference that it defines a region external to the orifice into which the cavity discharges during outflow. This region provides the equivalent of the "end-correction" to the oscillating mass in the orifice passage as in the classical treatment of the problem.

The model is sketched on figure 13. The field is divided into the free stream and a "wall jet" containing the flow processed through the cavity during the cycle by the streamline BSR_i and BSR_o, respectively, at the instant of extreme inflow and outflow. The dividing "lid" oscillates about the "hinge-point" (S) which is not fixed a-priori. The location of the hinge-point relative to the actual size of the orifice represents the decrease in the effective area of the active opening, a feature suggested by experimental observations of the flow.

The pressure perturbation acting on the opening of the resonator cavity is taken to be composed of two contributions: (1) the incident acoustic excitation, (P_i), and: (2) the aerodynamic pressure, (P_a), induced by the deflection of the free stream. The dimensionless mean velocities in the wall jet upstream and downstream of the cavity are taken to be characteristic parameters of the problem:

$$\eta_1 = \frac{u_1}{U_o} \; ; \; \eta_s = \frac{u_s}{U_o} \qquad (1)$$

Figure 13

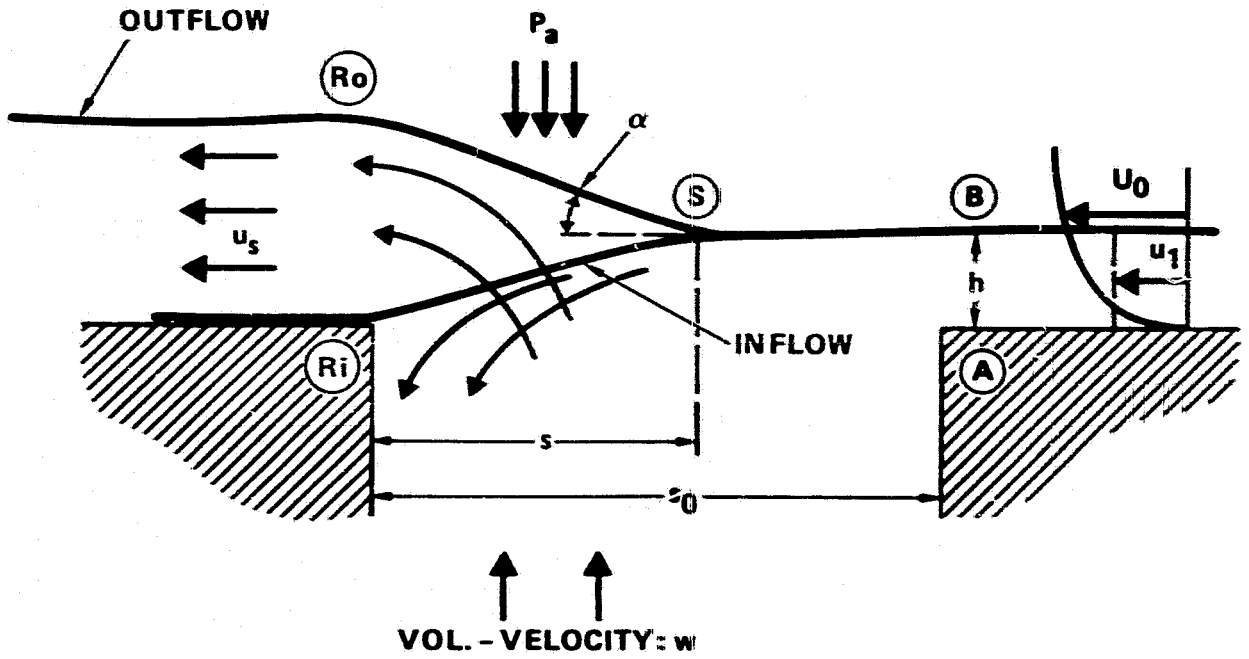

SCHEMATIC HINGED-LID MODEL

The first of these is related to the profile of the upstream boundary layer and is expected to be near unity. The second is expected to be significantly lower, but still of the order of unity. The difference between η_1 and η_s is related to the increase in the momentum thickness and the drag experienced by the mean flow in crossing the orifice.

Mass conservation reads, assuming incompressible flow and small deflections:

$$u_1 h = ws + U_o(h + s\alpha) + \frac{s^2}{2}\frac{d\alpha}{dt} \tag{2}$$

The pressure perturbation due to the deflection of the external flow is proportional to α, as in aerodynamic small perturbation theory

$$p_a = K\rho U_o^2 \alpha \tag{3}$$

Equations (2) and (3) can be integrated;

$$\langle p_a \rangle = K\rho U_o^2 \left(\frac{h}{s}\right)\left(\frac{\eta_1}{\eta_s} - 1\right) + \frac{K\rho U_o}{\eta_s}\left[\frac{1}{1 + \frac{j\omega s}{2u_s}}\right]\langle w \rangle \tag{4}$$

where $\langle\ \rangle$ denotes the complex representation of harmonic functions at frequency ω. The first term in equation 4 indicates that there is an acoustically induced constant pressure loading on the cavity. It is positive when the ratio of the characteristic velocities in the wall-jet upstream and downstream of the cavity, u_1/u_s is larger than unity, which is expected.

The equation governing the motion of an idealized "slug" of fluid in the orifice is written, as usual:

$$R_o s\langle w \rangle + \rho L\frac{d\langle w \rangle}{dt} = \langle p_i \rangle + \langle p_a \rangle - \langle p_c \rangle \tag{5}$$

where $\langle p_c \rangle$ is known as a function of $\langle w \rangle$ from the adiabatic compression relations and $\langle p_i \rangle$ is the external source of acoustic excitation. L is the equivalent length of the orifice. Combining these relations and

integrating, we obtain the components of the impedance:

$$\langle Z \rangle = \frac{\langle p_i \rangle}{\langle w \rangle_s} = R + jX \tag{6}$$

$$R = R_0 + \frac{K\rho U_0}{\eta_s s} \left[1 + \frac{\omega^2 s^2}{4u_s^2}\right]^{-1} \tag{7}$$

$$X = X_0 - \frac{K\rho\omega}{2\eta_s^2} \left[1 + \frac{\omega^2 s^2}{4u_s^2}\right]^{-1} \tag{8}$$

R_0 and X_0 are the components of the impedance without grazing flow as commonly defined.

The high speed behavior of those parameters turns out to be governed by a modified Strouhal number

$$St = \frac{\omega s}{u_s} = \frac{1}{\eta_s} \left(\frac{\omega s}{U_0}\right) \tag{9}$$

Note that this parameter is not yet calculable because the effective dimension of the slot, s, is not known. However, we can expect both s/s_0 and η_s to be of the order of unity. It follows that, for present data, the bracketed term can be set to one above U_0 = 10 m/s with good accuracy. The resistance should then increase linearly with the grazing velocity. The grazing flow introduces a negative inertance which is independent of the velocity, i.e. a reactance which is proportional to frequency.

The data provide two relations between the three parameters of the model. The slope of the resistance-velocity curve in the high grazing-velocity regime is

$$\frac{d\left(\frac{R-R_0}{\rho c^*}\right)}{dU_0} = \left(\frac{K}{\eta_s}\right) \frac{1}{sc^*} \tag{10}$$

The ratio of R to X (the phase angle of impedance vector) yields, without restriction to high grazing velocities:

$$-1/2 \frac{(R-R_0)}{(X-X_0)} \left(\frac{\omega s_0}{u_0}\right) = \eta_s \frac{s_0}{s} \qquad (11)$$

Inasmuch as K is a constant and η_s must be resonably constant, the key parameter of this model is the ratio (s_0/s), i.e., the "effective" dimension of the orifice.

We require an additional empirical relation to determine all the parameters. It is provided by measurements of the average pressure in the cavity. One must first recognize that the presence of the slot disturbes the boundary layer of the grazing flow even in the absence of the acoustic field. Measurements in steady flow (without excitation) yielded the following:

$$C_p\Big]_{\omega=0} = \frac{p_c - p_{bo}}{1/2\rho U_0^2} = 0.07 \pm .003 \qquad (12)$$

A very slight overpressure is developed in the cavity due to the disturbance caused by the slot, a result which is well known. When the acoustic excitation is turned on (100 Hz, 120 db) the mean cavity pressure increases very clearly as shown on figure 14, normalized by the root-mean-squared amplitude of the incident pressure. The increase should be associated with the time-independent term in equation 4.

In order to evaluate this term, one needs an expression for the height of the inflow-channel, (h/s).. It is defined by the geometry of the model at the extreme inflow position of the "lid"; equation 3 with $\alpha = -h/s$ is equated to the real value of $\langle p_a \rangle$ from equation 4 at the instant of maximum $\langle w \rangle$ $(t = 0)$. Making then the approximations appropriate to the high-speed regime one finds.

Figure 14

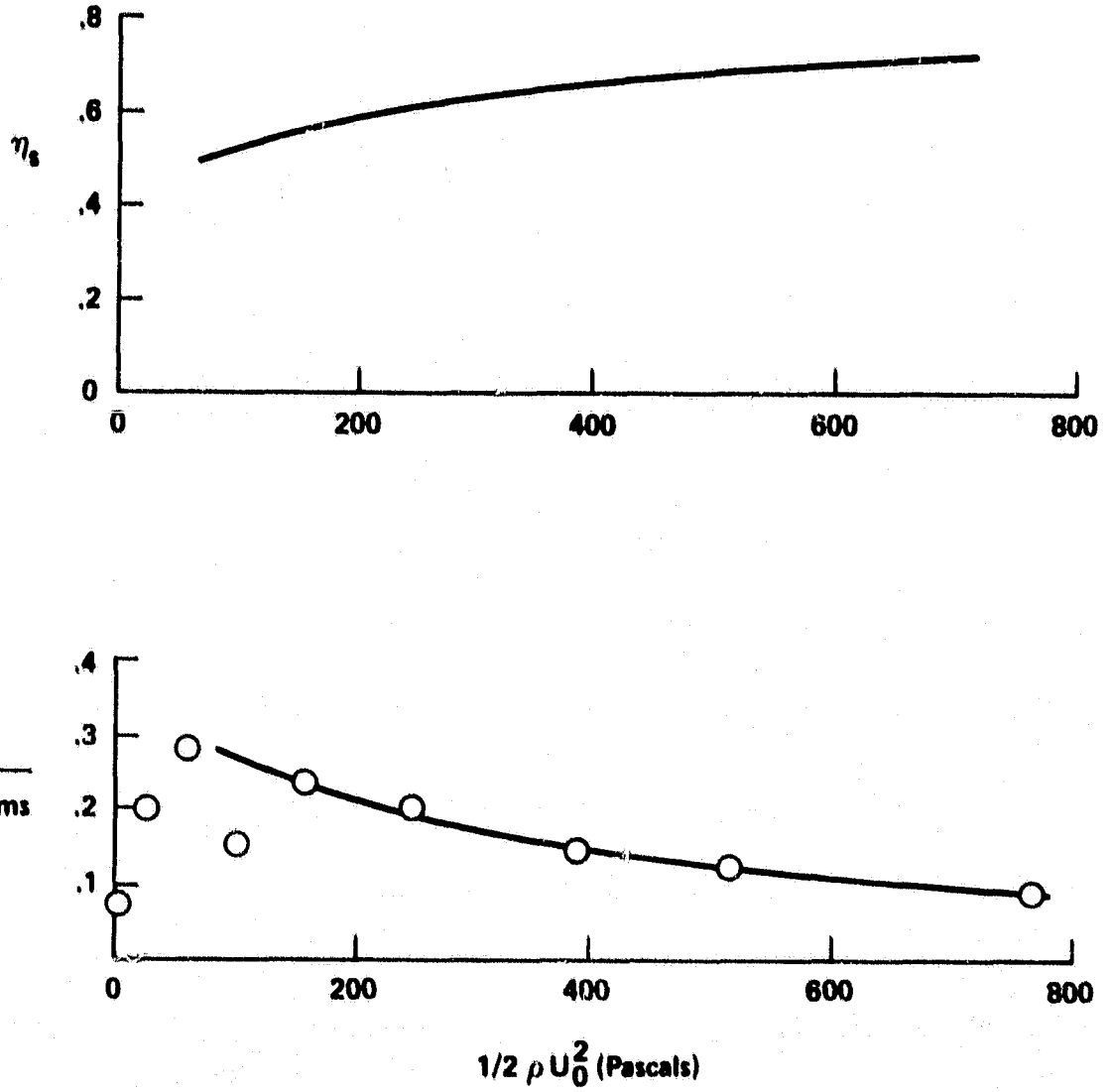

MEASUREMENTS AND CORRELATION OF THE
ACOUSTICALLY INDUCED MEAN CAVITY PRESSURE
(EXITATION: 100 Hz, 120 db)

$$\frac{h}{s} = \frac{p_{io}}{K\rho U_o^2}\,\frac{\eta_s}{\eta_1} \qquad (13)$$

$$R >> K \; ; \; R = \frac{K\rho U_o}{\eta_s^{\,s}} \; ; \; \frac{\omega s}{\eta_s U_\infty} << 1$$

It follows that

$$\frac{\overline{p_a}}{(\overline{p_i})_{rms}} = \sqrt{2}\left[\frac{\eta_1 - \eta_s}{\eta_1}\right] \qquad (14)$$

η_1 represents the profile of the upstream boundary layer. This is approximated in this model by the ratio of the average velocity in the inner layer, u_1, to the velocity at the edge of that layer. For power-profiles characteristic of turbulent boundary layers the ratio is simply

$$\eta_1 = \frac{U_1}{U_o} = \frac{U_1}{U_\infty}\,\frac{U_\infty}{U_o} = \left(\frac{n}{n-1}\right) \; ; \; \frac{U}{U_\infty} = \left(\frac{y}{\delta}\right)^{1/n} \qquad (15)$$

In our case the velocity distribution in the upstream boundary layer followed approximately the 1/5 power low, so that :

$$\eta_1 \approx .833 \qquad (16)$$

Using equations 13 and 15, η_s is determined and plotted on figure 14. It is found to be of exactly the order of magnitude expected. It decreases slightly with the grazing velocity. This trend is compatible with measurements of the change in momentum thickness of the boundary layer across the slot.

We can now return to equation (11) to evaluate (s_o/s). In addition to the data shown on figure 1, we have acoustic measurements at two different frequencies; The resistance of the resonator is not affected by it within the accuracy of the data, but the reactance varies significantly,

see figure 15. Unfortunately, we do not have measurements of the mean cavity pressure at 80 and 125 Hz; we shall assume in the following that the values of η_s determined at 100 Hz remain valid at the other frequencies.

The ratio s_0/s is plotted on figure 16. As the grazing velocity increases at a fixed excitation frequency s_0/s changes from less to more than unity, sketches illustrate the nature of this transition. At low grazing velocities, the influence of the jet from the resonator propagates upstream and causes a separation of the oncoming boundary layer ahead of the disturbance. At high velocities, the momentum of the grazing flow comes it further; The stagnation point in the boundary layer moves off the upstream wall into the free shear layer over the slot. This interpretation leads thus to distinguishing two entirely different regimes of the interaction: a regime of boundary layer separation and regime of free-jet interaction. Such categories of interaction have been identified before in connection with studies of transverse jets and free-jets impinging on one-another.

There are two scales in this problem. The geometry of a steady-state plume in a crosswind depends on w/U_0 which is proportional to $P_i/\rho U_0^2$. The relative convective time characterizing the unsteady nature of the flow is $\omega/(U_0/s)$. These suggest a dimensionless representation of the phemomena which is presented on figure 17. Indeed, it results in a very satisfactory collapse of all the velocity and frequency data to a single curve. Its asymptotic behavior at low grazing speeds (high Stranton number) is not clear for lack of sufficiently precise measurements. If the initial slope of the reactance velocity variation were zero, the curve would tend to a constant; if it is finite, the curve will diverge. Additional measurements are needed to clarify this and to verify the correlation in terms of its dependence on the excitation level.

In summary, the proposed model provides a coherent physical explanation of the effects of a grazing flow on the resistance as well

FIGURE 15

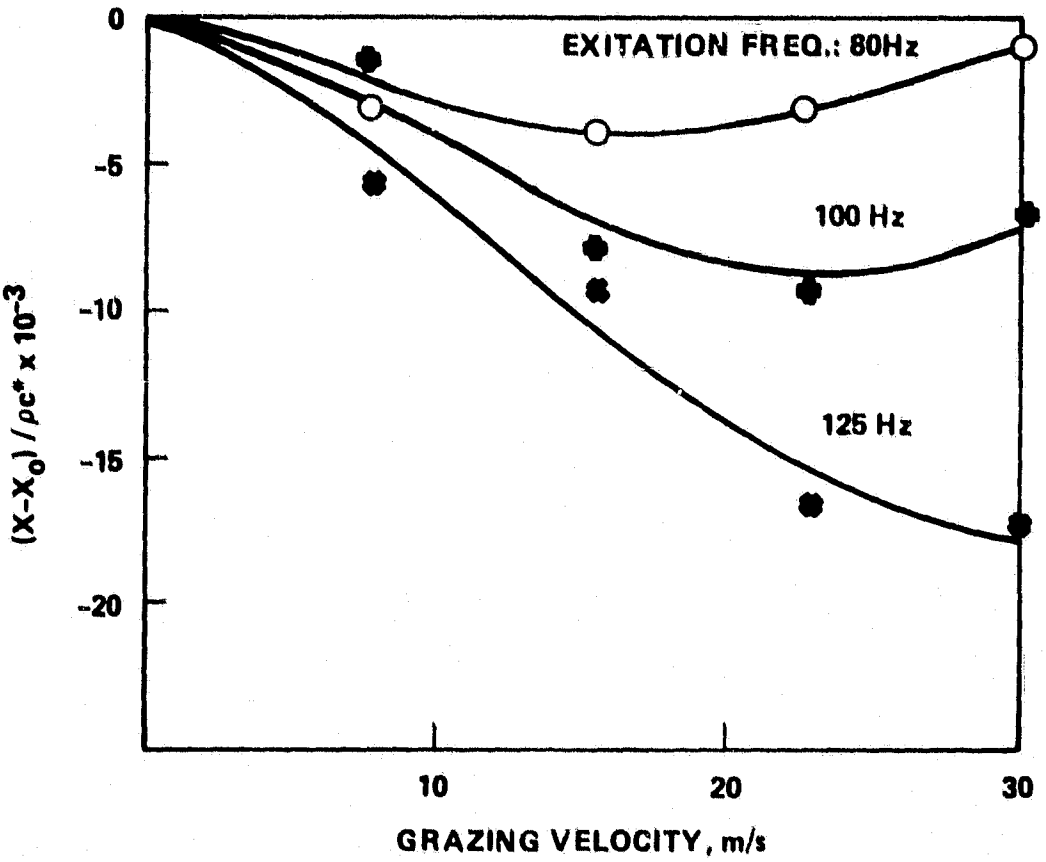

EFFECT OF THE GRAZING FLOW ON THE REACTANCE AT VARIOUS EXITATION FREQUENCIES

Figure 16

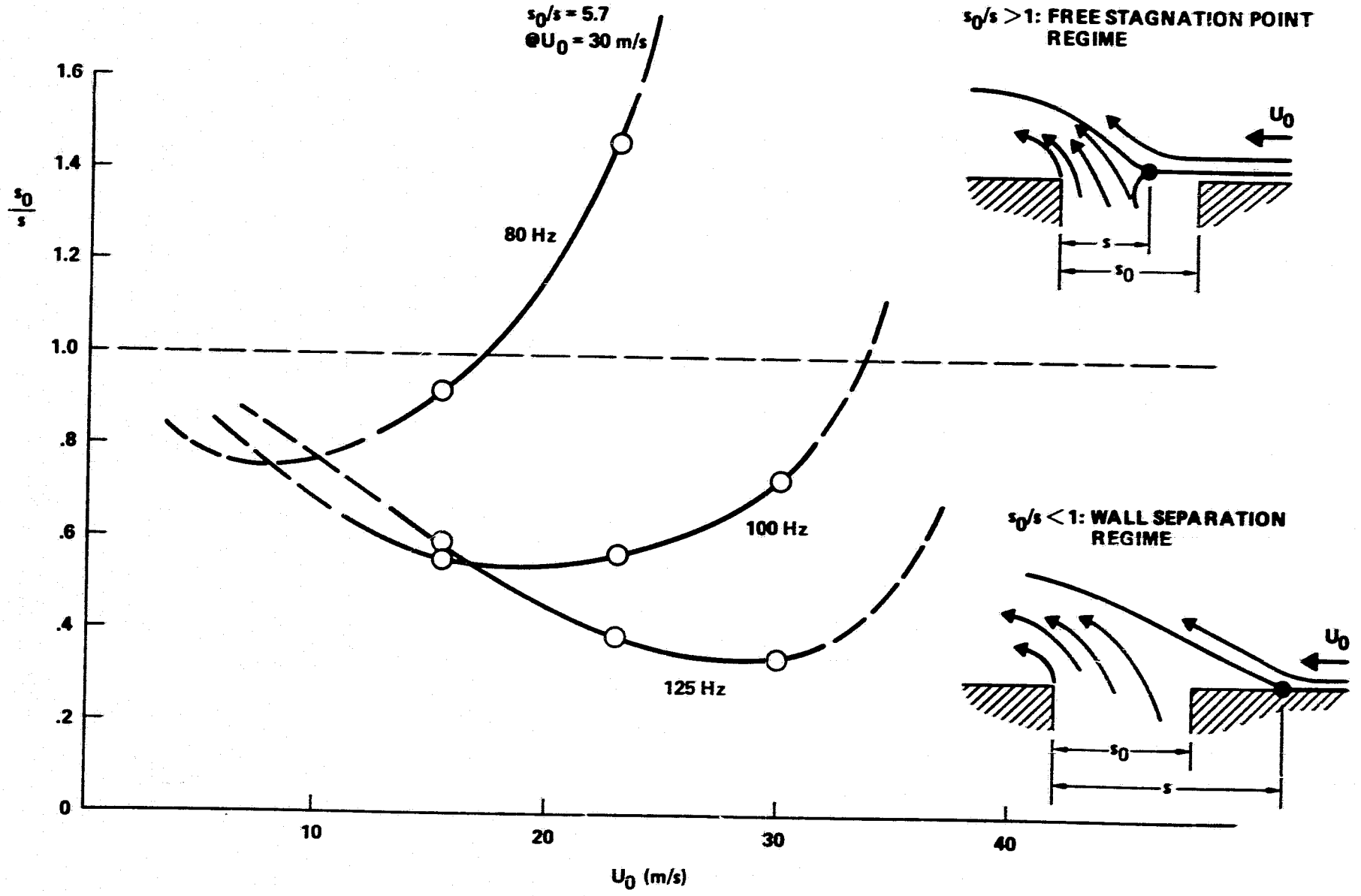

EFFECTIVE ORFICE AREA -- TWO REGIMES OF INTERACTION

Figure 17

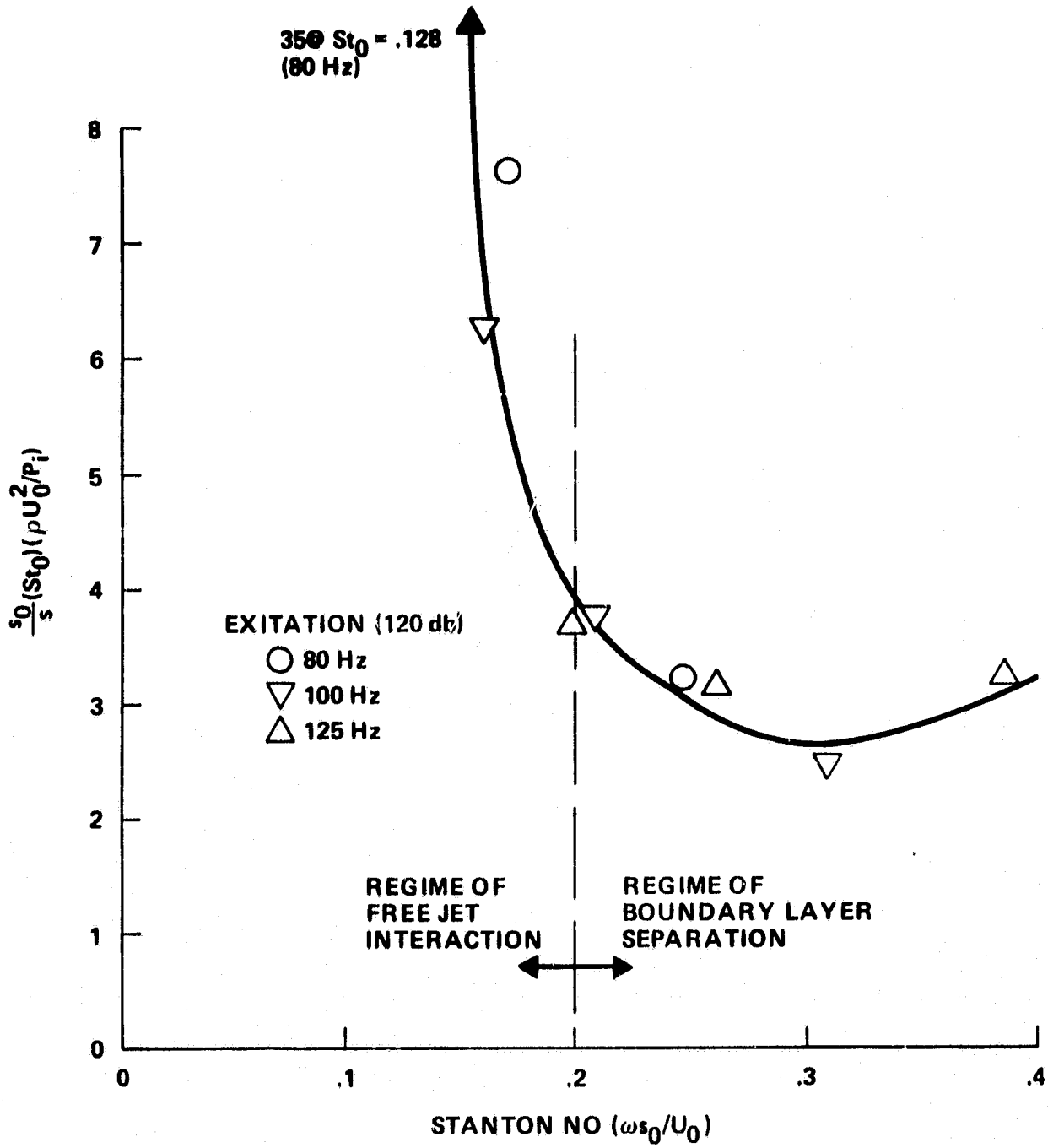

CORRELATION OF THE EFFECTIVE ORIFICE AREA FUNCTION

as on the reactance of Helmholtz resonators; it also yields scaling parameters which correlate the gross trends quite satisfactorily.

The increase in resistance is primarily associated with the deflection of the outer flow. The changes in the reactance are due to the delay in estabilishing the external plume in analogy with the "end-mass" correction commonly included in modeling acoustic resonators in a stationary environment. There are two distinct regimes of interaction with a grazing flow which determine the size of this "end-mass". In the first regime (high Stroudhal numbers) it appears to be modeled by the separation of the grazing boundary layer off the wall upstream of the disturbance (the inscipient separation problem). This regime is characterized by a gradual decrease in the reactance of the resonator with grazing velocity. A second, low Stroudhal number regime is established when the mode of interaction between the two perpendicular flows changes to a direct impingment at a stagnation point in the free shear layer over the orifice. At that transition the slope of the reactance with grazing velocity reverses.

The quantitative correlations developed in this paper pertain to a two-dimensional configuration. No structural difference between the two and the three dimensional cases is expected, but the magnitudes will undoubtedly differ. The model suggests mechanisms by which the influence of the upstream boundary layer may enter. This refinement is outside of the scope of the present model, but it does seem that no single correlation of boundary layer effects, valid for both regimes of interaction, is likely to be successful.

CONCLUSION

The primary objective of this experiment was to provide a description of the interaction between a grazing flow and the acoustically induced velocity-perturbations in the neighborhood of the orifice of a Helmholtz resonator. It was successful in that it yielded not only a base of quantitive data but also suggested a definite structure of the perturbation field which seems to lend itself to analytical modeling by the superposition of singularities on a steady grazing flow. Specifically the experimental data suggest that the interaction can be represented by the appearance of an oscillating vortex downstream of the orifice of the resonator.

In terms of the simple mechanical analogue of acoustic resonators, the grazing flow appears to introduce a time-variable "end-correction" to the oscillating mass coupling the cavity to the environment. This concept is used to modify the phenomenological "lid-model" discussed in the literature leading to a successful correlation of the observed behavior not only of the acoustic resistance but also of the reactance of the resonator.

ACKNOWLEDGMENT

This research was supported by a grant from NASA Lewis Research Center; we are particularily grateful for the encouragement and sustained support received from Dr. E. Rice, Head, Noise Abatement Section, who monitored this project. We also wish to acknowledge the interest and the helpful advice given us by Dr. Alan Hersh during the course of this work.

REFERENCES

1. Hersh, A.S. and Walker, B.E.:
   "Effect of Grazing Flow on the Acoustic Impedance of Helmholtz Resonators Consisting of Single and Clustered Orifices".
   NASA Contractors Report 3177 (Contract NAS3-19745)
   Lewis Research Center, August 1979

2. Kopenhans J., Ronneberger, D.:
   "The Acoustic Impedance of Orifices in the Wall of a Flow Duct with a Laminar or Turbulent Flow Boundary Layer
   AIAA Sixth Aeroacoustic Conference
   Hartford, Conn, June 1980

3. Baumeister, K.J. and Rice E.J.:
   "Visual Study of the Effect of Grazing Flow on the Oscillatory Flow in a Resonator Orifice"
   NASA Lewis Research Center
   Technical Memorandum TM X-3288, 1976

4. Ingard, K.V. and Labate, S.:
   "Acoustic Circulation Effects and the Nonlinear Impedance of Orifices"
   JASA 22, 211, 1950

5. Ingard, K.V. and Ising, H.:
   "Acoustic Nonlinearity of an Orifice"
   JASA, 42, 6, 1967

6. Rice, E.J.:

"A Theoretical Study of the Acoustic Impedance of Orifices in the Presence of a Steady Grazing Flow"
NASA Lewis Research Center
Technical Memorandum TM X-71903, 1976

7. Rogers T. and Hersh, A.S.:

"Effect of Grazing Flow on Steady-state Resistance of Isolated Squar Edged Orifices"
NASA Lewis Research Center

8. Walker, B.E. and Charwat, A.F.

"Experimental Mapping of the Flow Field Over a Helmholts Resonator in Grazing Flow: Compilation of Data", UCLA, Department of Mechanics and Structures Report 81-102, March 1981 (NASA Lewis Research Center Grant NSG 3236).

LIST OF SYMBOLS

c*: Velocity of sound

h: parameter for the lid-model (see fig. 12)

p: pressure

P_i : acoustic excitation pressure

P_c : pressure on the bottom of the cavity

P_d : pressure on the downstream face of the slot

P_s : pressure on the upstream face of the slot

ℓ: nominal thickness of orifice (see equ. 5)

R: acoustic resistance of the resonator

R_o : resistance with no grazing flow

s: streamwise dimension of slot (reference)

u: streamwise velocity (parallel to boundary)

U_o: free steam velocity of the grazing flow

w: crosstream velocity (normal to boundary)

x: streamwise coordinate (origin at the upstream corner of the slot)

X: acoustic reactance of the resonator

X_o : reactance with no grazing flow

y: crosstream coordinate (origin at the boundary)

ρ: density

η: parameter for the lid-model (see equ. 1)

ω: circular frequency of the acoustic excitation